Influence of Glutathione on the Oxidation of 1-Methyl-6-hydroxy-1,2,3,4-tetrahydro-β-carboline: Chemistry of Potential Relevance to the Addictive and Neurodegenerative Consequences of Ethanol Abuse

Qing-Ping Han and Glenn Dryhurst*

Department of Chemistry and Biochemistry, University of Oklahoma, Norman, Oklahoma 73019

Received July 3, 1995[⊗]

Recent evidence suggests that intraneuronal metabolism of ethanol by catalase/H_2O_2 and an ethanol-inducible form of cytochrome P450 together generate acetaldehyde and oxygen radicals including the hydroxyl radical ($HO^•$). Within the cytoplasm of serotonergic neurons, these metabolic processes would thus provide acetaldehyde, which would react with unbound 5-hydroxytryptamine (5-HT) to give 1-methyl-6-hydroxy-1,2,3,4-tetrahydro-β-carboline (**1**), known to be formed at elevated levels in the brain following ethanol drinking, and $HO^•$ necessary to oxidize this alkaloid. In this study, it is demonstrated that the $HO^•$-mediated oxidation of **1** at physiological pH yields 1-methyl-1,2,3,4-tetrahydro-β-carboline-5,6-dione (**8**) that reacts avidly with free glutathione (GSH), a significant constituent of axons and nerve terminals, to give diastereomers of 8-*S*-glutathionyl-1-methyl-1,2,3,4-tetrahydro-β-carboline-5,6-dione (**9A** and **9B**). In the presence of free GSH, ascorbic acid, other intraneuronal antioxidants/reductants, and molecular oxygen diastereomers, **9A**/**9B** redox cycle in reactions that generate H_2O_2 and, via trace transition metal ion catalyzed decomposition of the latter compound, $HO^•$. Further reactions of **9A**/**9B** with GSH and/or $HO^•$ generate several additional glutathionyl conjugates that also redox cycle in the presence of intraneuronal reductants and molecular oxygen forming H_2O_2 and $HO^•$. Thus, intraneuronal formation of **1** and $HO^•$ as a consequence of ethanol drinking and resultant endogenous synthesis of **8**, **9A**, and **9B** would, based on these *in vitro* chemical studies, be expected to generate elevated fluxes of H_2O_2 and $HO^•$ leading to oxidative damage to serotonergic axons and nerve terminals and the irreversible loss of GSH, both of which occur in the brain as a consequence of ethanol drinking. Furthermore, deficiencies of 5-HT and loss of certain serotonergic pathways in the brain have been linked to the preference for and addiction to ethanol.

Ethanol drinking results in formation of a number of tetrahydroisoquinoline (TIQ)[1−3] and tetrahydro-β-carboline (THβC)[4] alkaloids in dopamine (DA)- and 5-hydroxytryptamine (5-HT)-rich regions of the brain, respectively. Furthermore, infusions of certain TIQs and THβCs into specific brain regions augment volitional ethanol drinking by the rat.[5−8] Such evidence supports the hypothesis that acetaldehyde, the proximate metabolite of ethanol, condenses with brain indolamines and catecholamines to form THβCs and TIQs, respectively, that might contribute to the addictive properties of the fluid.[9,10] Other lines of evidence suggest that deficiencies of 5-HT[11−15] and DA[13,16,17] in specific brain regions also augment ethanol drinking. Furthermore, prolonged exposure of animals and humans to ethanol results in neuronal loss[18−20] including certain serotonergic, dopaminergic, and noradrenergic pathways.[21] Thus, ethanol-induced degeneration of specific serotonergic and catecholaminergic pathways in the brain might, therefore, be a factor linked to the addictive properities of the fluid.

Available evidence indicates that TIQ and THβC alkaloids formed (or suspected of being formed) in the brain following ethanol drinking are short-lived species *in vivo* although their fates are largely unknown.[22] Recent investigations, however, have established that these TIQs and THβCs are very easily oxidized compounds.[23−25] Accordingly, it is not inconceivable that once formed in the brain these alkaloids are rapidly oxidatively metabolized and that the resulting metabolites might contribute to the degeneration of serotonergic and catecholaminergic pathways and in the activation of the opioid system which also appears to play an important role in compulsive ethanol drinking.[26−30] An important impetus to the idea that significant levels of TIQ and THβC alkaloids might be formed and then oxidized in the brain as a consequence of drinking derives from reports that ethanol is intraneuronally metabolized to acetaldehyde by catalase/H_2O_2[31] and an ethanol-inducible form of cytochrome P450.[32,33] The latter isoform is a potent generator of oxygen radicals including the hydroxyl radical ($HO^•$).[34,35] These results indicate that intraneuronal mechanisms are available to metabolize ethanol to acetaldehyde that would be expected to react with cytoplasmic (*i.e.* unbound) biogenic amine neurotransmitters to form TIQ and THβC alkaloids. Formation of $HO^•$ as a byproduct of these reactions provides an *in situ* mechanism to oxidize these intraneuronal alkaloids.

Acute and chronic ethanol drinking also evoke a significant decrease in brain levels of glutathione (GSH) with little or no corresponding increase in the oxidized tripeptide (GSSG) although the activities of enzymes associated with GSH biosynthesis are increased.[33,36] These observations suggest that drinking results in an accelerated and irreversible loss of brain GSH, perhaps by reactions with endogenous substances such as oxidized forms of ethanol-dependent TIQ and THβC alkaloids. One such alkaloid is 1-methyl-6-hydroxy-1,2,3,4-

* To whom correspondence should be addressed.
[⊗] Abstract published in *Advance ACS Abstracts,* March 1, 1996.

0022-2623/96/1839-1494$12.00/0

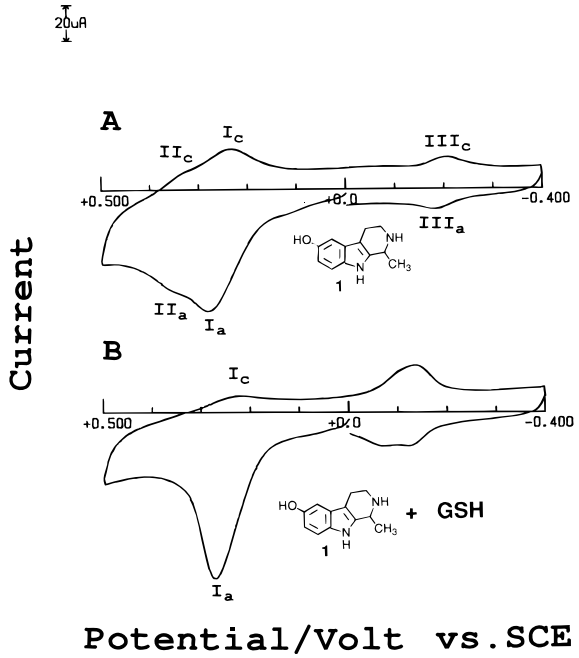

Figure 1. Cyclic voltammograms at the PGE of (A) 0.25 mM **1** and (B) 0.25 mM **1** plus 1.5 mM GSH in pH 7.4 phosphate buffer ($\mu = 1.0$). Sweep rate: 200 mV s^{-1}.

Scheme 1

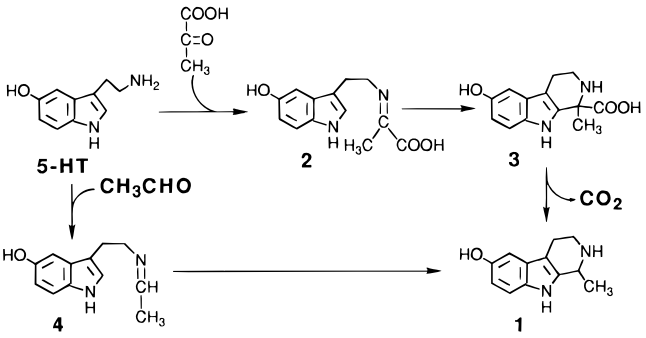

tetrahydro-β-carboline (**1**). This alkaloid occurs as a normal but ultratrace constituent of the mammalian brain and other tissue, probably by reaction between pyruvate and 5-HT to give Schiff base **2** that cyclizes to **3** and subsequently decarboxylates (Scheme 1).[37,38] However, experiments with the rat have shown that dietary ethanol potentiates formation of **1** in the brain presumably by reaction of acetaldehyde with 5-HT to give Schiff base **4** that cyclizes to give the alkaloid (Scheme 1).[4] Urinary excretion of **1** by humans is elevated during ethanol intoxication and declines during detoxification.[37,38] In the event that **1** is indeed oxidized in the cytoplasm of serotonergic axon terminals, the reaction would necessarily occur in the presence of GSH.[39] Accordingly, this communication describes the influence of GSH on the electrochemically-driven, enzyme- and $HO^{\bullet}$-mediated oxidation chemistry of **1**.

Results

Electrochemical and Enzymatic Oxidation of 1 in the Presence of GSH. Cyclic voltammetry of **1** (0.25 mM) in pH 7.4 phosphate buffer at a sweep rate (ν) of 200 mV s^{-1} shows two overlapping oxidation peaks I_a ($E_p = 270$ mV) and II_a ($E_p \approx 350$ mV) on the initial anodic sweep (Figure 1A). After scan reversal, reduction peaks II_c ($E_p = 335$ mV) and I_c ($E_p = 233$ mV) form reversible couples with oxidation peaks II_a and I_a, respectively. At more negative potentials, reduction peak III_c ($E_p = -203$ mV) forms a reversible couple with oxidation peak III_a ($E_p = -184$ mV) that appears on the second anodic sweep. An earlier investigation[24] established that, at potentials corresponding to the rising segment of peak I_a, **1** is oxidized (1e, $1H^+$) to radical **5** that dimerizes to **7** (Scheme 2). However, at more positive potentials a further one electron is abstracted from radical **5** to give an intermediate represented by the cationic resonance structures **6a** and **6b** (Scheme 2). Nucleophilic addition of **1** to **6** provides a second route to dimer **7**.[24] However, nucleophilic addition of water to **6** also occurs to give the 5,6-dihydroxy-THβC **8R** that, at peak I_a potentials, is immediately oxidized (2e, $2H^+$) to dione **8**. Peak I_c observed in cyclic voltammograms of **1** (Figure 1A) corresponds to reduction of **6** to **1**. Peak II_a is due to oxidation of dimer **7**, formed in the peak I_a reaction, to an intermediate that is responsible for reduction peak II_c. Dione **8** is reduced to **8R** at peak III_c, and peak III_a corresponds to the reverse reaction.[24]

In the presence of increasing concentrations of GSH (0.25−2.5 mM) a number of changes occur in cyclic voltammograms of **1** (0.25 mM). Thus, the peak II_a/peak II_c couple is eventually eliminated and the peak current (i_p) for reduction peak I_c is significantly decreased (Figure 1B). However, a reversible couple remains in the same potential region as peaks III_c and III_a, but the peak currents for this couple increase significantly.

Figure 2A presents a chromatogram of the product solution formed following a controlled potential electrooxidation of **1** (0.25 mM) at 200 mV in pH 7.4 phosphate buffer for 30 min at 22 °C. Under these conditions dimer **7** is the major product along with much smaller yields of purple dione **8** that coelutes with unreacted **1**.[24] In the presence of a 3-fold molar excess of GSH but under otherwise identical experimental conditions, formation of dimer **7** is completely blocked and the major product is the 5-*S*-glutathionyl conjugate of **1**, *i.e.* **10**, along with smaller yields of diastereomers **9A** and **9B** (Figure 2B). With increasingly positive applied potentials the rate of oxidation of **1** increases and the yields of **10** initially increase (Figure 2C, 400 mV) and then decrease (Figure 2D, 600 mV; Figure 2E, 800 mV). By contrast, the yields of diastereomers **9A** and **9B** increase with more positive applied potentials such that at 800 mV they represent the major reaction products (Figure 2E). The results shown in Figure 2B−E suggest that one route to **9A** and **9B** results from oxidation of glutathionyl conjugate **10**. This was confirmed by controlled potential electrooxidations of **10** (0.25 mM) at applied potentials ≥ 400 mV in the presence of GSH (0.75 mM) at pH 7.4 which resulted in formation of equimolar concentrations of **9A** and **9B** as the sole reaction products (data not shown).

Previous studies[24] demonstrated that several enzyme systems (peroxidase VI/H_2O_2, tyrosinase/O_2, ceruloplasmin/O_2) also oxidize **1** to **7** and **8** at pH 7.4. The influence of GSH on these enzyme-mediated oxidations of **1** were essentially identical to those observed in the electrochemically-driven reaction. To illustrate, Figure 3 presents chromatograms of the product solutions formed following incubation of **1** (0.25 mM) with peroxidase VI (10 units mL^{-1}), H_2O_2 (0.5 mM and 1.5 mM), and GSH (0.75 mM) for 5 min at 22°C. Thus, the major reaction products were **9A**, **9B** and **10** along with very

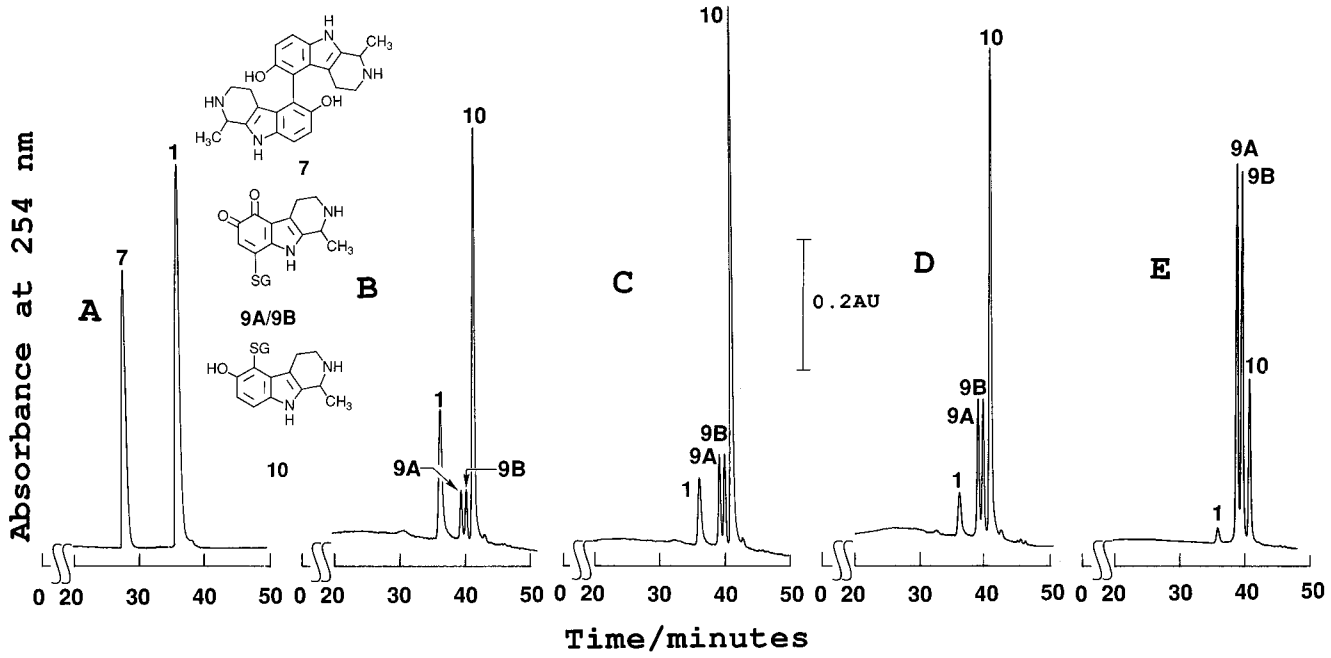

Figure 2. HPLC chromatograms of the product solutions obtained following controlled potential electro-oxidation of (A) 0.25 mM **1** at 200 mV; (B−E) 0.25 mM **1** plus 0.75 mM GSH at (B) 200 mV, (C) 400 mV, (D) 600 mV, and (E) 800 mV in phosphate buffer ($\mu = 0.2$). All reactions were terminated after 30 min. Chromatography employed HPLC method I. Injection volume: 6.0 mL.

Scheme 2

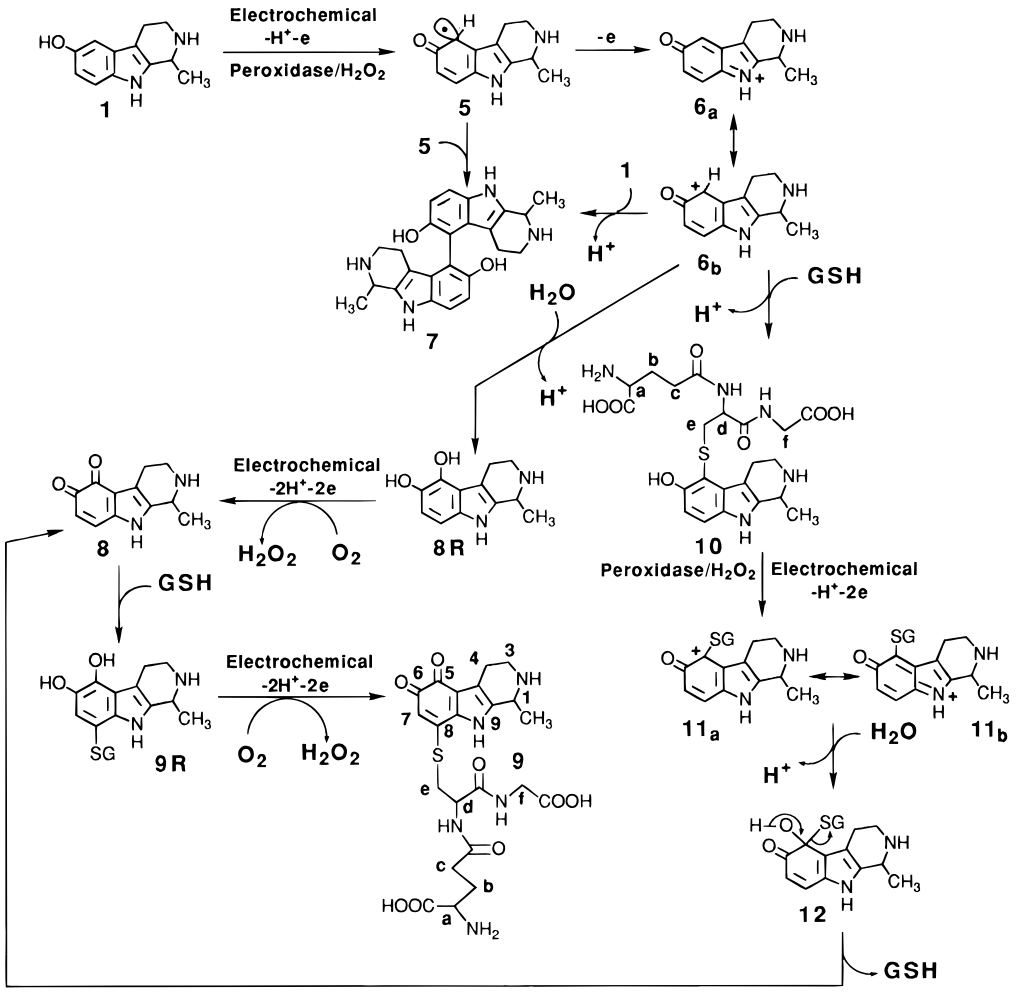

minor yields of **15**. Furthermore, the yields of **10** decreased and those of **9A** and **9B** increased with increasing concentrations of H_2O_2. The trace concentrations of **15** formed in the peroxidase/H_2O_2-mediated oxidation of **1** in the presence of GSH resulted from secondary reactions of **9A** and **9B** that are dependent on the presence of molecular oxygen (see later discussion). Electrochemical oxidations were performed in the

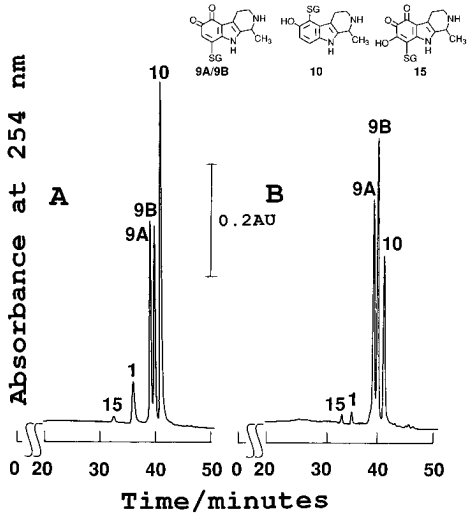

Figure 3. HPLC chromatograms of the product solutions obtained following incubation of **1** (0.25 mM) with peroxidase VI (10 units mL^{-1}), GSH (0.75 mM) and (A) 0.5 mM H_2O_2 or (B) 1.5 mM H_2O_2 in pH 7.4 phosphate buffer ($\mu = 0.2$) at 22 °C for 5 min. Chromatography employed HPLC method I. Injection volume: 6.0 mL.

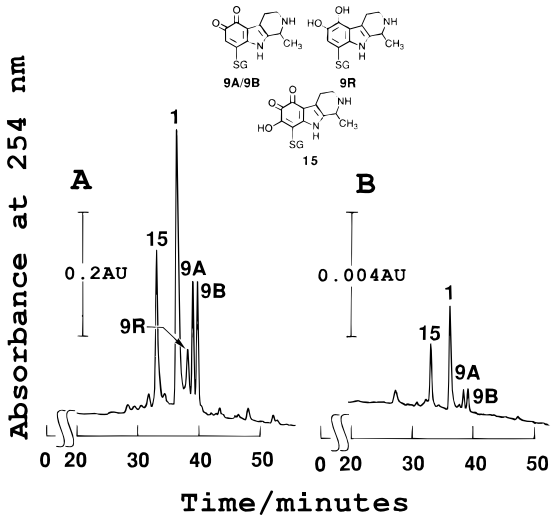

Figure 4. HPLC chromatograms of the product solutions obtained following incubation of (A) 0.25 mM **1** and (B) 2.5 μM **1** with GSH (0.75 mM), Fe^{2+} (200 μM), Na_2 EDTA (240 μM), ascorbic acid (1.0 mM) and H_2O_2 (1.0 mM) in pH 7.4 phosphate buffer ($\mu = 0.2$) at 22 °C for 5 min. Chromatography employed HPLC method I. Injection volume: 6.0 mL.

absence of molecular oxygen, hence accounting for the absence of **15** in the resultant product mixtures.

Hydroxyl Radical (HO•)-Mediated Oxidation of 1 in the Presence of GSH. Oxidation of **1** (0.25 mM) with an HO•-generating system (200 μM Fe^{2+}/240 μM Na_2EDTA/1.0 mM ascorbic acid/1.0 mM H_2O_2; see the Experimental Section for details and the order of addition of reagents) at pH 7.4 and 22 °C was extremely rapid. The initially colorless solution instantaneously turned a pink/purple color upon addition of the final reagent, H_2O_2. However, within approximately 10 min a dark brown, presumably polymeric, precipate appeared. HPLC analysis (method I) of the initially-formed pink/purple solution revealed that dione **8** was the major reaction product although several additional minor, unstable, and therefore unidentified products were formed. Figure 4A shows a chromatogram of the product solution formed immediately following the HO•-mediated oxidation of **1** (0.25 mM) in the presence of

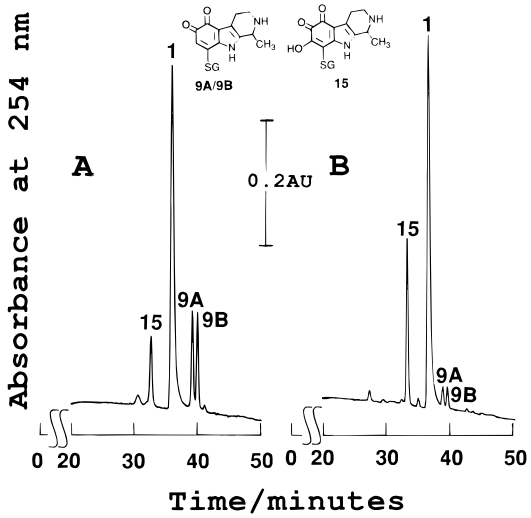

Figure 5. HPLC chromatograms of the product solution obtained following incubation of **1** (0.25 mM) with GSH (0.75 mM), Fe^{2+} (200 μM), Na_2 EDTA (240 μM) and ascorbic acid (1.0 mM) in pH 7.4 phosphate buffer ($\mu = 0.2$) at 22 °C in the absence of added H_2O_2 for (A) 12 h and (B) 24 h. Chromatography employed HPLC method I. Injection volume: 6.0 mL.

GSH (0.75 mM) at pH 7.4 and 22 °C. Under these experimental conditions the major reaction products are **9A**, **9B**, and **15** with smaller yields of **9R**. Dione **8**, dimer **7**, and glutathionyl conjugate **10** were not formed as detectable products in this reaction. Oxidation of much lower concentrations of **1** (2.5 μM) in the presence of GSH (0.75 mM) by the same HO•-generating system also gave **9A**, **9B**, and **15** as the major initial products along with traces of **9R** (Figure 4B). In the absence of added H_2O_2, oxidations of **1** (0.25 mM) in the presence of GSH (0.75 mM), Fe^{2+} (200 μM), Na_2EDTA (240 μM), and ascorbic acid (1.0 mM) were relatively slow. However, within 30 min **9A** and **9B** could be chromatographically detected as products. Within 12 h, **9A** and **9B** were the major products along with slightly lower yields of **15** (Figure 5A). After 24 h levels of **9A** and **9B** had decreased significantly and yields of **15** correspondingly increased (Figure 5B).

Reactions of Dione 8 and Glutathionyl Conjugates 9A and 9B with GSH. The electrochemically-driven, peroxidase/H_2O_2- and HO•-mediated oxidations of **1** in the presence of GSH at physiological pH all gave diastereomeric glutathionyl conjugates **9A** and **9B** as significant reaction products. However, **15** was not formed in the electrochemically-driven reactions (Figure 2B−E) which were always carried out in the absence of molecular oxygen. Very small yields of **15** were detected among the initial products of the peroxidase/H_2O_2-mediated oxidations (Figure 3) which were carried out in the presence of molecular oxygen. Furthermore, the yields of **15** increased when the initial product solution was stirred in the presence of molecular oxygen while those of **9A**/**9B** correspondingly decreased (data not shown). By contrast, **15** was a major initial product of the HO•-mediated oxidation of **1** in the presence of GSH (Figures 4 and 5). The structures of conjugates **9A** and **9B** suggested that they are formed by a direct reaction between dione **8** and GSH. The observations summarized above and the structure of **15** (to be discussed subsequently) further suggest that this compound is formed by HO• attack on **9A**/**9B**. In order to investigate such reactions in more detail, samples of **8** were prepared by controlled potential electrooxidation of **1**

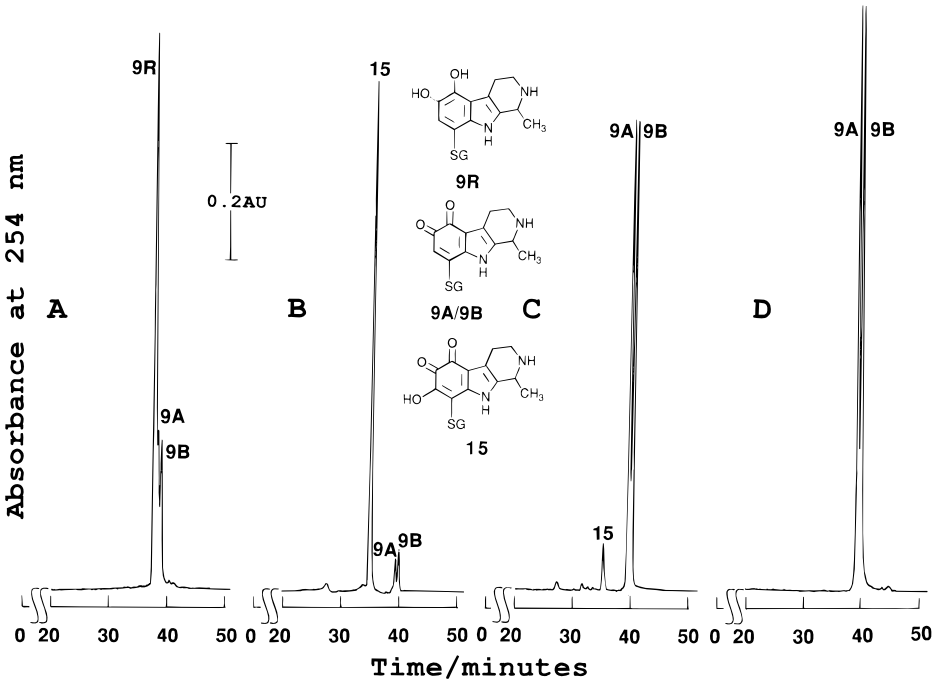

Figure 6. HPLC chromatograms of the product solutions obtained following reaction of 0.6 mM **8** with GSH (2.0 mM) in pH 7.4 phosphate buffer ($\mu = 0.2$) at 22 °C (A) for 15 min, (B) for 2 h, (C) for 2 h in the presence of 0.55 mM mannitol and (D) for 2 h in the presence of 5.5 mM mannitol. Chromatography employed HPLC method I. Injection volume: 2.0 mL.

(0.25 mM) at pH 1.5 using a very positive applied potential (1.0 V). Under these conditions **1** is almost quantitatively oxidized to **8** (*ca*. 95%) with only minor yields of dimer **7**.[24] Pure solutions of **8** were prepared by preparative HPLC of the product mixture (method II) when the dione eluted at $t_R = 24$ min. When a thoroughly deoxygenated solution of **8** (*ca*. 0.6 mM) dissolved in the HPLC mobile phase (pH 3.0) was adjusted to pH 7.4 and reacted with GSH (2.0 mM) at 22 °C, the initial purple color of the dione ($\lambda_{max} = 540$, 350, 238 nm) rapidly faded. The spectrum of the resultant colorless product solution ($\lambda_{max} = 310$, 238 nm) was that of **9R**. This was confirmed by HPLC analysis (method II; t_R for **9R** = 24 min) and the fact that cyclic voltammetry of this product in the mobile phase (pH 3.0) exhibited a reversible couple at $E^{\circ\prime} = -35$ mV which was identical to that of **9A** and **9B** under identical conditions. Furthermore, controlled potential electrooxidation of **9R** dissolved in the HPLC mobile phase ($\lambda_{max} = 308$, 236 nm) at 200 mV for 10 min gave an equimolar mixture of **9A** and **9B** ($\lambda_{max} = 550$, 346, 248 nm).

Incubation of **8** (0.6 mM) with GSH (2.0 mM) at pH 7.4 and 22 °C in the presence of molecular oxygen resulted in the initial formation of **9R** along with smaller yields of **9A** and **9B** (Figure 6A). However, with time, the yields of these products decreased and, correspondingly, **15** appeared and ultimately became the major product (Figure 6B). When the HO• scavenger mannitol (0.55 mM) was incubated with **8** (0.6 mM) and GSH (2.0 mM) at pH 7.4 and 22 °C in the presence of molecular oxygen the yield of **15** was very significantly reduced (Figure 6C). Higher concentrations of mannitol (5.5 mM) completely blocked formation of **15**, and the only reaction products were **9A** and **9B** in equimolar yield (Figure 6D).

In the absence of molecular oxygen, incubations of **9A**/**9B** (total concentration 0.6 mM) with GSH (2.0 mM) at pH 7.4 and 22 °C gave **9R**. By contrast, in the presence of molecular oxygen, **9A**/**9B** were almost completely transformed into **15** within 1−2 h. Again, the presence of mannitol (0.55 mM) decreased the yield of **15** after 2 h by approximately 90%, and higher concentrations (5.5 mM) of the HO• scavenger completely blocked formation of **15**. Taken together the preceding evidence indicates that HO• is generated when **8** or **9A**/**9B** are incubated with GSH in the presence of molecular oxygen at pH 7.4 and that this radical is responsible for formation of **15** from **9A**/**9B**. Attempts to isolate and spectroscopically elucidate the structure of **15** were unsuccessful owing to the decomposition of this compound during the final freeze-drying step. However, addition of a large molar excess of GSH (≥2.5 mM) to a freshly chromatographed solution of **15** (*ca*. 0.25 mM, HPLC method I) adjusted to pH 7.4 resulted in the initial formation of **17R** and **17** (Figure 7A). Ultimately, **15** was quantitatively transformed into **17** under these experimental conditions (Figure 7B,C). Compounds **17** and **17R** could be isolated (see the Experimental Section). On the basis of the structures of **9A**/**9B** and **17** and that fact that **15** is clearly an intermediate between these compounds whose formation was dependent upon HO•, the only plausible structure for **15** is 8-*S*-glutathionyl-7-hydroxy-1-methyl-1,2,3,4-tetrahydro-β-carboline-5,6-dione.

Redox Cycling Properties of 9A/9B. The preceding results indicated that dione **8** reacts avidly with free GSH at physiological pH in the presence of molecular oxygen to give, initially, **9R** and thence **9A** and **9B** and that the latter diastereomers subsequently transform into **15** as a result of HO• formation. As noted earlier, **9A**/**9B** are readily reduced by excess free GSH. Furthermore, following controlled potential electroreduction of **9A**/**9B** at −300 mV in deoxygenated pH 7.4 phosphate buffer the resultant **9R** was rapidly oxidized to an equimolar mixture of **9A** and **9B** when the solution was exposed to atmospheric oxygen. A cyclic voltammogram ($\nu = 100$ mV s^{-1}) of **9A**/**9B** at pH 7.4 exhibits a single reduction peak ($E_p = -228$ mV) on the initial cathodic sweep corresponding to the 2e, 2H$^+$ reduction of these conjugates to **9R** (Figure 8). After scan reversal a reversible oxidation peak ($E_p = -212$ mV) corresponds

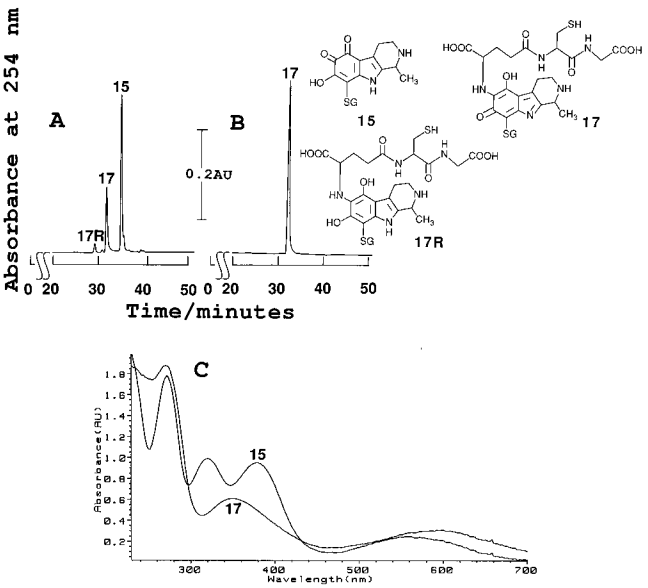

Figure 7. HPLC chromatograms of the product solutions obtained following reaction of **15** (*ca*. 0.25 mM) with GSH (2.5 mM) in pH 7.4 phosphate buffer at 22 °C for (A) 2 h and (B) 4 h. (C) UV−visible spectra of **15** (0.25 mM) and of the product solution formed 4 h after addition of GSH (2.5 mM), *i.e.* **17**. Chromatography employed HPLC method I. Injection volume: 2.0 mL.

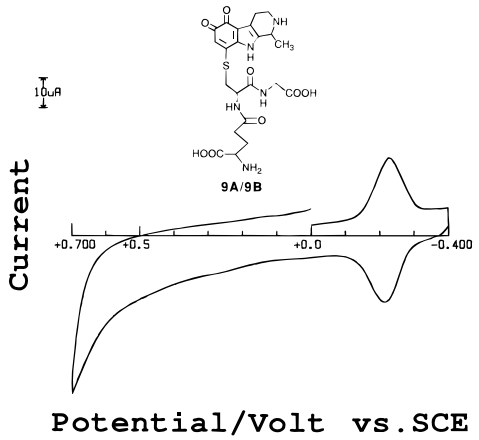

Figure 8. Cyclic voltammogram at the PGE of 0.40 mM **9A**/**9B** in pH 7.4 phosphate buffer ($\mu = 1.0$). Sweep rate: 100 mV s^{-1}.

to the reverse reaction. Cyclic voltammograms of pure samples or **9A**/**9B** were identical to that of the 1:1 mixture of these diastereomers presented in Figure 8. Taken together, the above information and the fact that $E^{\circ\prime}$ values for cellular reductants lie in the range −400 to −500 mV *vs* NHE[40] (−158 to −258 mV *vs* SCE) suggested that the **9A**/**9B**/**9R** couple ($E^{\circ\prime} = -220$ mV at pH 7.4) should redox cycle in the presence of such agents and molecular oxygen. This was explored by incubating **9A**/**9B** with representative cellular reductants in air-saturated pH 7.4 phosphate buffer at 37 °C and comparing the initial rates of oxygen consumption (measured with a Clark-type oxygen electrode system) to those measured in the absence of these conjugates (Table 1). Indeed, incubation of **9A**/**9B** (equimolar, total concentration 50 μM) with GSH, NADPH, L-cysteine (CySH), or ascorbic acid (1.0 mM) at 37 °C resulted in significant increases in the initial rates of oxygen consumption. Addition of catalase to a solution of **9A**/**9B** (50 μM) and GSH (1.0 mM) that had been incubated for 5 min in the reaction chamber of the oxygen

Table 1. Effects of **9A**/**9B** on the Initial Rate of Oxygen Consumption by Physiological Reductants at pH 7.4 and 37 °C

concn of **9A**/**9B**/ μM[a]	reductant	concn of reductant/ mM	initial rate of oxygen consumption/nmol of oxygen min^{-1}
0	GSH[c]	1.0	0.61 ± 0.02
50		1.0	13.1 ± 0.6
0	CySH[c]	1.0	0.32 ± 0.02
50		1.0	6.5 ± 0.2
0	NADPH[c]	1.0	0.62 ± 0.2
50		1.0	5.2 ± 0.2
0	ascorbic acid[c]	1.0	0.75 ± 0.05
50		1.0	92.7 ± 1.3

[a] 25 μM **9A** plus 25 μM **9B**. [b] Measurements made with a micro oxygen electrode assembly. Volume of solution in the oxygen electrode chamber: 600 μL. Values reported are mean ± standard deviation for at least three replicate measurements. [c] In pH 7.4 phosphate buffer ($\mu = 0.2$).

Table 2. Influence of Catalase, Superoxide Dismutase, Transition Metal Ions, Complexing Agents, and HO• Scavengers on the Initial Rates of Oxygen Consumption by the **9A**/**9B**/GSH Redox Cycling System at pH 7.4 and 37 °C

redox cycling[a] system	added compound	initial net rate of oxygen consumption[b]/ nmol of oxygen min^{-1}
9A/**9B** (50 μM)/ GSH (1.0 mM)	none	12.5 ± 0.6[c]
	catalase (0.2 mg)	5.2 ± 0.2
	SOD (200 units)[d]	11.7 ± 0.4
	Fe^{2+} (10 μM)[e]	38.0 ± 1.2
	(100 μM)[e]	52.3 ± 1.2
	Fe^{3+} (10 μM)[f]	26.1 ± 0.9
	(100 μM)[f]	35.3 ± 0.8
	Cu^{2+} (10 μM)[g]	39.0 ± 1.0
	(100 μM)[g]	60.0 ± 4.0
	DTPA (1 mM)[h]	3.9 ± 0.3
	ethanol (1 mM)	3.2 ± 0.1
	(10 mM)	2.0 ± 0.1
	mannitol (1 mM)	2.6 ± 0.2
	(10 mM)	1.3 ± 0.1

[a] Reactants were dissolved in 600 μL of air-saturated pH 7.4 phosphate buffer ($\mu = 0.2$) in the chamber of a micro oxygen electrode assembly thermostated at 37 °C. [b] Initial net rates of oxygen consumption were the difference in the rate measured in the presence of **9A**/**9B** and that measured in the absence of **9A**/**9B**. [c] Reported rates are the mean ± standard deviation for at least three replicate experiments. [d] Superoxide dismutase. [e] Added as $Fe(NH_4)_2(SO_4)_2 \cdot 6H_2O$. [f] Added as $FeCl_3$. [g] Added as $CuSO_4$. [h] Diethylenediaminepentaacetic acid.

electrode system resulted in the liberation of 42.1 ± 0.2% of the consumed oxygen. This indicates that the redox cycling reactions of **9A**/**9B**/**9R** result in the reduction of molecular oxygen to H_2O_2. This was confirmed by incubating catalase with **9A**/**9B** (50 μM) and GSH (1.0 mM) at pH 7.4 and 37 °C which resulted in a 50% decrease in the initial rate of oxygen consumption compared to that measured in the absence of this enzyme (Table 2). However, addition of catalase to the **9A**/**9B**/GSH solution in the oxygen electrode chamber after 10 min resulted in the liberation of only 15.0 ± 0.1% of the consumed oxygen, indicating that H_2O_2 was being consumed by secondary reactions, *i.e.* decomposition to HO• (hence leading to formation of **15**). Superoxide dismutase (SOD) had virtually no effect on the initial rate of oxygen consumption by the **9A**/**9B**/GSH system, indicating that superoxide anion radical ($O_2^{\bullet -}$), even if formed, had no significant influence on the redox cycling reactions. By contrast, trace levels of added transition metal ions (Fe^{2+}, Fe^{3+}, Cu^{2+}) significantly increased the initial rate of oxygen consumption whereas the transition metal ion complexing agent diethylenetriaminepentaacetic acid (DTPA) and HO• scavengers

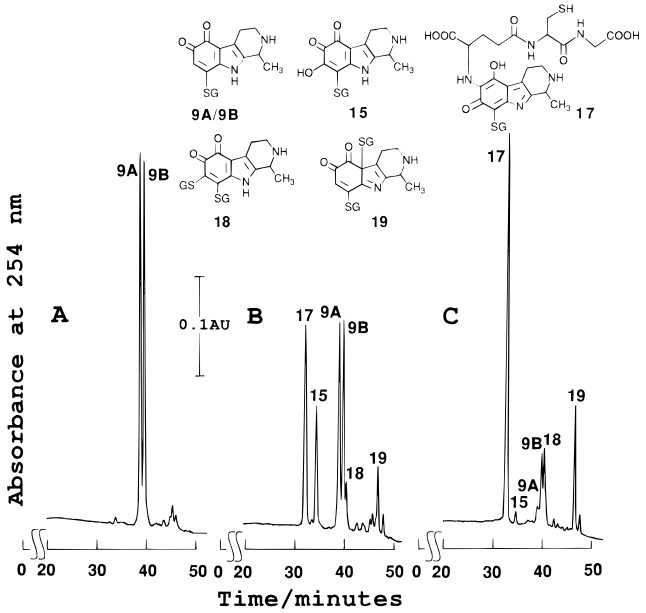

Figure 9. HPLC chromatograms of a solution initially containing **9A**/**9B** (50 μM) and GSH (1.0 mM) in pH 7.4 phosphate buffer (μ = 0.2) at 37 °C that was stirred and exposed to the atmosphere (A) immediately after preparation, (B) after 10 min and (C) after 2 h. Chromatography employed HPLC method I. Injection volume: 10.0 mL.

(mannitol, ethanol) had the opposite effect (Table 2). Taken together, these results indicate that H_2O_2, the major byproduct of the **9A**/**9B**/GSH/O_2 redox cycling system, is indeed decomposed by trace concentrations of transition metal ions, that always contaminate the buffer system employed, to generate HO$^\bullet$ and, furthermore, that this radical potentiates the reactions involved.

Figure 9 presents a series of chromatograms of the product solutions formed at various times after **9A**/**9B** (50 μM) and GSH (1.0 mM) were incubated at 37 °C in air-saturated pH 7.4 phosphate buffer. These chromatograms reveal that, in addition to redox cycling processes (Table 1), several other chemical reactions occur. Thus, after 20 min approximately 50% of **9A**/**9B** has disappeared and **15**, **17**, **18**, and **19** in addition to several other minor unidentified products were formed (Figure 9B). After 2 h, almost no **9A**/**9B** and **15** remained and the major product was **17** along with much smaller yields of **18** and **19**. Methods were developed to optimize formation of the bi-*S*-glutathionyl conjugates **18** and **19** (which could be resolved into diastereomers **19A** and **19B** using HPLC method III) such that they could be isolated in sufficient quantities to permit spectroscopic structure elucidation (see the Experimental Section). Chromatographic analysis of the product mixture formed throughout the course of the reaction between **9A**/**9B** (50 μM) and GSH (1.0 mM) at pH 7.4 and 37 °C revealed that **15** was the initial major product. However, with time the yields of **15** decreased and, correspondingly, **17** appeared and became the major product, confirming that **15** is the precursor of **17**.

Redox Cycling Properties of 17. A cyclic voltammogram (ν = 200 mV s^{-1}) of **17** at pH 7.4 exhibited two reversible reduction processes at $E^{o\prime}$ = −148 and −456 mV (Figure 10). Addition of excess GSH or ascorbic acid (4 mM) to the bright blue solution of **17** (0.2 mM; λ_{max} = 586, 340, 274 nm) in pH 7.4 phosphate buffer resulted

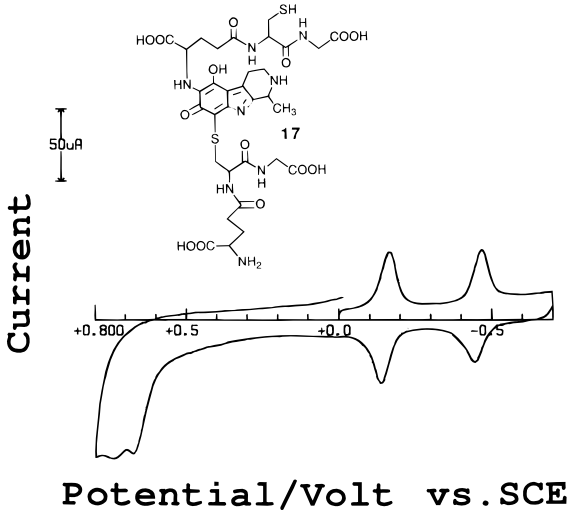

Figure 10. Cyclic voltammogram at the PGE of 0.4 mM **17** in pH 7.4 phosphate buffer (μ = 1.0). Sweep rate: 200 mV s^{-1}.

in formation of a colorless solution of **17R** (λ_{max} = 334, 300, 262 sh nm). Interestingly, controlled potential electroreduction of **17** at pH 7.4 using applied potentials of −200 or −500 mV, *i.e.* corresponding to the first and second voltammetric reduction peaks of **17**, respectively (Figure 10), both resulted in formation of **17R**. Exposure of this solution of **17R** to the atmosphere led to the initial development of a green color (λ_{max} = 604, 364, 274 nm) that subsequently transformed into blue **17** within a few minutes. Cyclic voltammetry (ν = 200 mV s^{-1}) of the partially autoxidized (green) solution of **17R** showed a reversible reduction process at $E^{o\prime}$ = −152 mV corresponding to the first reversible reduction process observed in cyclic voltammograms of **17** (Figure 10). Although details of the redox chemistry of **17** remain to be elucidated, the preceding observations suggested that this compound should also redox cycle in the presence of GSH or other cellular reductants and molecular oxygen. Indeed, **17** (50 μM) significantly increased the initial rates of oxygen consumption by GSH, ascorbic acid, CySH, and NADPH (1.0 mM) in air-saturated pH 7.4 phosphate buffer at 37 °C (Table 3). Addition of catalase after **17** had been incubated with GSH for 5 min in the oxygen electrode chamber resulted in the liberation of 44 ± 3% of the consumed oxygen; this decreased to 8 ± 0.2% when catalase was added after 10 min. Both DTPA (10 mM) and mannitol (10 mM) decreased the initial rate of oxygen consumption by the **17** (50 μM)/GSH (1.0 mM) system by 18 ± 0.8 and 15 ± 0.6%, respectively. Together, these results indicate that the redox cycling of **17**/**17R** generates H_2O_2 as a byproduct that is subsequently decomposed by trace transition metal contaminants to HO$^\bullet$ and that this radical potentiates these reactions.

Periodic HPLC analysis (method III) of a solution of **17** (50 μM) in pH 7.4 phosphate buffer (μ = 0.2) maintained at 37 °C revealed that this compound was very slowly hydrolyzed to **15**. For example, after 6 h under these conditions approximately 8% of **17** was hydrolyzed to **15**.

Redox/Redox Cycling Properties of 15, 18, and 19. Cyclic voltammograms (ν = 100 mV s^{-1}) of **15**, **18**, and **19A**/**19B** at pH 7.4 are presented in Figure 11. Thus, **15** and **18** exhibit reversible reduction processes at $E^{o\prime}$ = −447 mV (**15**/**15R** couple) and −487 mV (**18**/**18R** couple), respectively (Figure 11A,B). Diastereo-

Table 3. Effects of **17**, **18**, and **19A/19B** on the Initial Rates of Oxygen Consumption by Physiological Reductants at pH 7.4 and 37 °C[a]

compound (concentration, μM)	reductant (concentration, mM)	initial rate of oxygen consumption/ nmol of oxygen min^{-1}
–	GSH (1.0)	0.61 ± 0.02
17 (50)		6.40 ± 0.20
18 (50)		1.00 ± 0.10
19A/19B (50)		1.30 ± 0.04
–	ascorbic acid (1.0)	0.75 ± 0.05
17 (50)		58.2 ± 0.8
18 (50)		5.5 ± 0.2
19A/19B (50)		7.8 ± 0.1
–	CySH (1.0)	0.32 ± 0.02
17 (50)		5.1 ± 0.2
18 (50)		1.2 ± 0.1
19A/19B (50)		2.6 ± 0.1
–	NADPH (1.0)	0.62 ± 0.2
17 (50)		8.6 ± 0.3
18 (50)		2.1 ± 0.1
19A/19B (50)		4.1 ± 0.1

[a] In pH 7.4 phosphate buffer (μ = 0.2). [b] Measurement were made with a micro oxygen electrode assembly. Volume of solution in the oxygen electrode chamber: 600 μL. Values reported are the mean ± standard deviation for at least three replicate measurements.

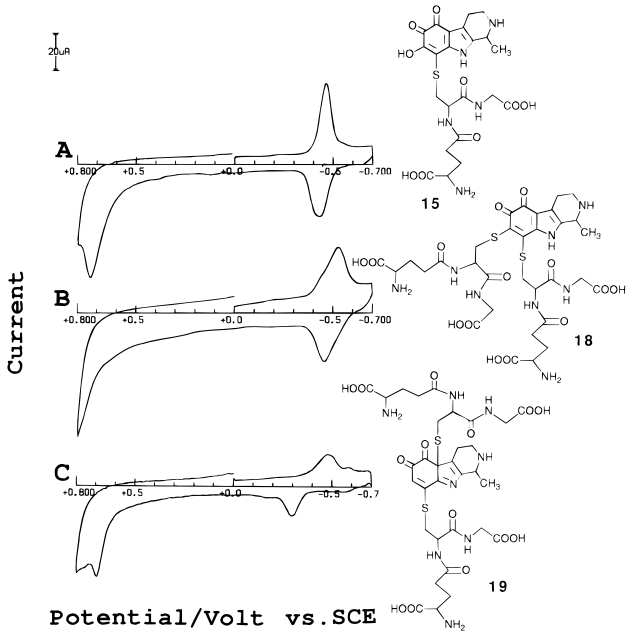

Figure 11. Cyclic voltammograms at the PGE of *ca*. 0.4 mM (A) **15**, (B) **18** and (C) **19A/19B** in pH 7.4 phosphate buffer (μ = 1.0). Sweep rate: 100 mV s^{-1}.

mers **19A** and **19B** both exhibited one major reduction peak (E_p = −485 mV) followed by a smaller reduction peak (E_p = −560 mV) on the initial cathodic sweep (Figure 11C). After scan reversal an oxidation peak (E_p = −295 mV) appears to form a quasi-reversible couple with the reduction peak at E_p = −485 mV. Incubations of **18** or **19A/19B** (50 μM) with ascorbic acid (1.0 mM) at pH 7.4 and 37 °C evoked a significant increase in the initial rate of oxygen consumption (Table 3). However, incubations of **18** or **19A/19B** (50 μM) with GSH, CySH, or NADPH (1.0 mM) evoked only rather modest increases in the rates of oxygen consumption (Table 3). These results indicate that **18** and **19A/19B** are not as effective redox cycling agents as **9A/9B** and **17**. It is probable that this is so because of the significantly more negative reduction potentials for **18**, **19A/19B** compared to **9A/9B** and **17**.

Discussion

Elimination of the peak II_a/peak II_c couple in cyclic voltammograms of **1** at pH 7.4 in the presence of free GSH (Figure 1B) suggests that the tripeptide blocks formation of dimer **7** in the peak I_a oxidation reaction. This was confirmed by analysis of the products of controlled potential electrooxidation of **1** in the presence of GSH which revealed that very little **7** is formed (Figure 2B). The peak current for peak I_c was also significantly decreased in the presence of GSH (Figure 1B), suggesting that putative intermediate **6**, formed in the peak I_a oxidation of **1**, is rapidly scavenged by GSH. The 5-*S*-glutathionyl conjugate **10** would be the expected product of the latter reaction, and indeed, this compound was the major product of the low potential (200 mV) controlled potential electrooxidation of **1** in the presence of GSH (Figure 2B). It appears that nucleophilic addition of GSH to **6** to give **10** (Scheme 2) is a very facile reaction that effectively blocks coupling of **1** and **6** to give dimer **7**. The small peak III_c/peak III_a couple ($E^{o\prime}$ = −196 mV) observed in cyclic voltammograms of **1** at pH 7.4 in the absence of GSH (Figure 1A) and the results of controlled potential electrooxidations of **1** at low applied potentials both indicate that dione **8** is a relatively minor reaction product.[24] In the presence of free GSH, **8** is scavenged by the tripeptide to give small, equimolar yields of the diastereomeric glutathionyl conjugates **9A** and **9B** (Figure 2B) by the pathway shown in Scheme 2. However, controlled potential electrooxidations of **1** in the presence of GSH result in decreased yields of **10** and increased yields of **9A/9B** as the applied potentials were made more positive (Figure 2B−E). This effect results from the fact that **10** is itself easily electrochemically oxidized at pH 7.4 (E_p = 310 mV; ν = 100 mV s^{-1}). Furthermore, controlled potential electrooxidations of **10** at applied potentials ≥ 600 mV at pH 7.4 both in the absence and presence of free GSH yielded **9A** and **9B** as the sole products. Thus, it can be concluded that at these potentials **10** is initially electrooxidized (2e, 1H$^+$) to putative cationic intermediate **11** that, following addition of water, gives **12** (Scheme 2). Subsequent elimination of a GSH moiety forms dione **8** that reacts with the free tripeptide to give **9A** and **9B**.

On the basis of the initial products formed, **9A**, **9B**, and **10** (Figure 3), it can be concluded that the peroxidase/H_2O_2-mediated oxidation of **1** in the presence of GSH follows the same *chemical* pathway as the electrochemically-driven reaction. The observation that the yields of **9A** and **9B** increase while those of **10** decrease with increasing concentrations of H_2O_2 is consistent with the conclusion that **10** is also oxidized by the peroxidase/H_2O_2 system by the same pathway proposed for the electrochemically-driven reaction (Scheme 2).

In the absence of GSH, the HO$^\bullet$-mediated oxidation of **1** at pH 7.4 yields dione **8** as the major reaction product. On the basis of pathways that have been proposed for the HO$^\bullet$-mediated oxidations of structurally-related compounds,[41,42] the initial step leading to **8** is probably attack by HO$^\bullet$ on **1** to give radical **13** (Scheme 3). While **8** was the major product of the HO$^\bullet$-mediated oxidation of **1**, several more minor, unstable, and therefore unidentified products were formed suggesting that HO$^\bullet$ also attacks other sites presumably forming additional radical intermediates. Further

Scheme 3

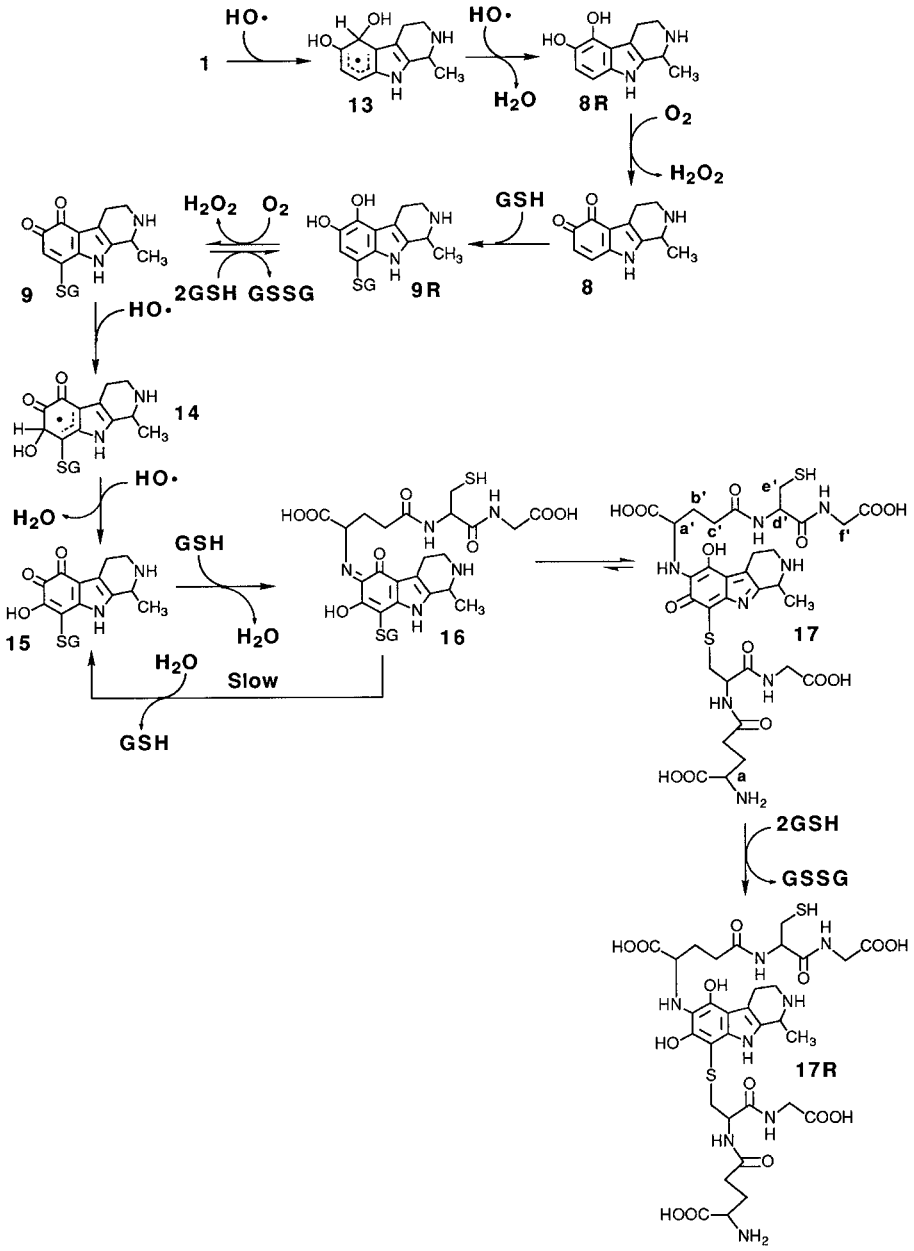

oxidation of **13** by HO• then gives the 5,6-dihydroxy-THβC, **8R**, that is very readily oxidized by molecular oxygen to **8**. In the presence of GSH (0.75 mM) the initial products detected as a result of the HO•-mediated oxidation of **1** (0.25 mM) at 22 °C are **9A**, **9B**, **9R**, and **15** (Figure 4A). Interestingly, the HO•-mediated oxidation of very low concentrations of **1** (2.5 μM) in the presence of a 300-fold molar excess of GSH under otherwise identical conditions also gave the same initial products (Figure 4B). Furthermore, incubation of **1** and GSH with Fe^{2+}/Na_2 EDTA/ascorbic acid and molecular oxygen in the absence of added H_2O_2 also resulted in the formation of **9A**, **9B**, and **15** (Figure 5). In the latter system H_2O_2, and hence HO•, are generated *in situ* as a byproduct of autoxidation of GSH and ascorbic acid.

The results discussed in connection with Figure 6 indicated that when **1** was incubated with a 3-fold molar excess of GSH at pH 7.4 and 22 °C the initial products formed were **9R**, **9A**, and **9B** which are subsequently transformed into **15**. Under similar conditions **9A** and **9B** are also transformed into **15**. The ability of mannitol to inhibit and, at sufficiently high concentrations, to completely block formation of **15** in these systems clearly indicates that HO• is responsible for formation of the latter conjugate from **9A** and **9B**. Taken together, these results indicate that **9R**, formed as a result of nucleophilic addition of GSH to dione **8**, must be oxidized by molecular oxygen to give initially **9A** and **9B** forming H_2O_2 (perhaps by intermediary formation of $O_2^{\bullet-}$ that rapidly dismutes) as a byproduct. Decomposition of H_2O_2 by trace levels of transition metal ion contaminants then provides the source of HO• necessary to convert **9A**/**9B** into **15**. On the basis of the structure of **15** (and **17**/**17R**) it appears probable that HO• initially attacks the C(7) position of **9A**/**9B** to give putative radical **14** that is oxidized by a second HO• to give **15** (Scheme 3). At 22 °C **15** reacts only slowly with a large molar excess of GSH to give **17** (Figure 7). A plausible reaction that leads to **17** involves condensation of the primary amine residue of GSH with the C(6) carbonyl group of **15** to give Schiff base glutathionyl conjugate **16**. This conjugate would be expected to be rather unstable in aqueous solution and, hence, probably exists predominantly as the tautomer **17**. The very slow

hydrolysis of **17** to **15** at pH 7.4 probably proceeds *via* Schiff base tautomer **16** (Scheme 3).

The $E^{o\prime}$ for **8**/**8R** (−196 mV at pH 7.4) is such that this couple would be expected to redox cycle in the presence of cellular reductants and molecular oxygen. However, the reaction of **8** with GSH to give **9R** and thence **9A** and **9B** is so facile it is unlikely that this dione would exist for significant periods of time in the presence of the tripeptide. Nevertheless, the **9A**/**9B**/**9R** system ($E^{o\prime}$ = −220 mV at pH 7.4) redox cycles efficiently in the presence of GSH, CySH, NADPH, and ascorbic acid (Table 1) to generate H_2O_2 as a byproduct (Table 2). The influence of transition metal ions, DTPA, mannitol, and ethanol on the rate of the redox cycling processes clearly support the conclusion that HO•, formed by subsequent transition metal ion catalyzed decomposition of H_2O_2, potentiates these redox cycling reactions (Table 2). One role of HO• in this respect is probably oxidation of **9R**. As discussed previously, a second role of HO• involves hydroxylation of **9A**/**9B** to give **15**. At 22 °C the latter conjugate is the most structurally complex product formed when **1** is oxidized by HO• in the presence of a relatively small (*i.e.* 3-fold) molar excess of GSH (Figures 4 and 5). Similarly, incubations of dione **8** or **9A**/**9B** with a 3-fold molar excess of free GSH in the presence of molecular oxygen at 22 °C also gave **15** as a major reaction product (Figure 6B). Further reaction of **15** with GSH to give **17** even in the presence of a large excess of the tripeptide at 22 °C is relatively slow (Figure 7). However, incubations of **9A**/**9B** with a large (20-fold) molar excess of GSH at 37 °C in the presence of molecular oxygen result not only in redox cycling reactions that generate H_2O_2 and hence HO• and **15** but also, under these conditions, in reactions of GSH with the latter compound to give **17** and with **9A**/**9B** to give **18** and **19** (Figure 9). A summary of the overall reaction chemistry involved is presented in Scheme 4. Thus, initial reduction of **9A**/**9B** by GSH yields **9R** that is subsequently oxidized by molecular oxygen forming H_2O_2 as a byproduct hence establishing the primary redox cycling reaction. Traces of transition metal ion contaminants (*e.g.* Fe^{2+}, maintained in its reduced form by free GSH) then decompose H_2O_2 to give HO• which potentiates the rate of this redox cycling reaction (Table 2) by oxidizing **9R** to **9A**/**9B**. However, HO• also attacks **9A**/**9B** to give **15** which, particularly at 37 °C in the presence of large molar excesses of GSH, reacts further to give **17**. The latter conjugate is also reduced by GSH to **17R** which is then oxidized by molecular oxygen generating H_2O_2 and thence HO•, thus establishing a second redox cycling system. Again, the rate of this redox cycling reactions is potentiated by HO• (Table 3), presumably as a result of oxidation of **17R** by this radical. The redox characteristics of **15**/**15R** ($E^{o\prime}$ = −447 mV at pH 7.4) suggest that this couple should also redox cycle in the presence of GSH, other cellular reductants, and molecular oxygen. However, the inability to isolate **15** precluded detailed studies with this compound. Nucleophilic addition of GSH to **9A**/**9B** results in the formation of minor amounts of the 5,6-dihydroxy-bi-*S*-glutathionyl conjugates **18R** and **19R** (Scheme 4). Autoxidation of these very easily oxidized compounds (Figure 11B,C) then leads to formation of **18** and **19A**/**19B**, respectively, H_2O_2, and HO•. Both **18** and **19A**/**19B** redox cycle particularly when incubated with ascorbic acid and molecular oxygen (Table 3), thus establishing yet additional mechanisms for H_2O_2 and HO• generation.

Metabolism of ethanol by catalase/H_2O_2[31] and an ethanol-inducible form of cytochrome P450[32,33] together provide routes for the intraneuronal formation of acetaldehyde, HO•, and other oxygen radical species. Within the cytoplasm of serotonergic axons and nerve terminals, these metabolic pathways would provide both the acetaldehyde required for the endogenous synthesis of **1** (Scheme 1), and HO• which would oxidize this THβC to dione **8** (Scheme 3). The facile reaction of **8** with GSH, known to be present at significant concentrations in the cytoplasm of axons and nerve terminals throughout the brain,[39] would then be expected to lead to the endogenous formation of **9A** and **9B** (Scheme 3). The results of this investigation, however, reveal that several quite different oxidizing systems oxidize **1** to **9A** and **9B** in the presence of free GSH. Accordingly, it appears reasonable to conclude that once **1** is formed intraneuronally as a result of ethanol drinking[4] subsequent oxidation of this easily oxidized alkaloid[24] would result in formation of **9A** and **9B** regardless of the oxidizing system responsible. A rather significant observation is that **1** is oxidized by HO• (the most probable intraneuronal oxidant[32,33]) even in the presence of very large molar excesses of GSH (Figure 4B). Indeed, *in vitro*, GSH fails to protect **1** against oxidation by either a rapid burst of high concentrations of HO• (Figure 4A,B) or the slow generation of much lower concentrations of this radical formed by transition metal ion mediated decomposition of the H_2O_2 resulting from autoxidation of GSH and ascorbic acid (Figure 5). These results appear to challenge the rather widely held belief that GSH, present in cells, including neurons, provides protection against the cytotoxic effects of HO•.

Formation of **8** and thence **9A** and **9B** in the cytoplasm of serotonergic neurons as a result of intraneuronal ethanol metabolism would, based on the results of this investigation, have a number of *chemical* consequences of potential relevance to known effects of acute and chronic ethanol drinking. Thus, in the presence of GSH, ascorbic acid, other intraneuronal antioxidants/reductants, and molecular oxygen, **9A**/**9B** would redox cycle in reactions that generate H_2O_2 (Tables 1 and 2; Scheme 4), perhaps at concentrations that exceed the detoxifying capacities of protective enzymes (catalase and GSH peroxidase). Even very low cytoplasmic concentrations of low molecular weight Fe^{2+} species, estimated to be approximately 0.1 μM,[43] are clearly sufficient to catalyze the decomposition of H_2O_2 to generate elevated fluxes of cytotoxic HO•. Furthermore, reactions of **9A** and **9B** with HO• and/or free GSH would together be expected to lead to secondary products such as **15** and **17**−**19**, all of which could establish additional redox cycling systems (Scheme 4) further potentiating H_2O_2 and HO• formation. Endogenous formation of these redox cycling systems and elevated fluxes of H_2O_2, HO•, and perhaps $O_2^{\bullet-}$ in addition to the HO• generated by ethanol metabolism[32,33] would together be expected to inflict neuronal damage by mechanisms that include lipid peroxidation. Indeed, both acute and chronic ethanol drinking result in marked increases in lipid peroxidation in the brain[33,44,45] although specific neuronal pathways that sustain this damage are presently unknown. The reaction pathways conceptualized in Schemes 3 and 4 predict that the HO•-mediated oxida-

Scheme 4

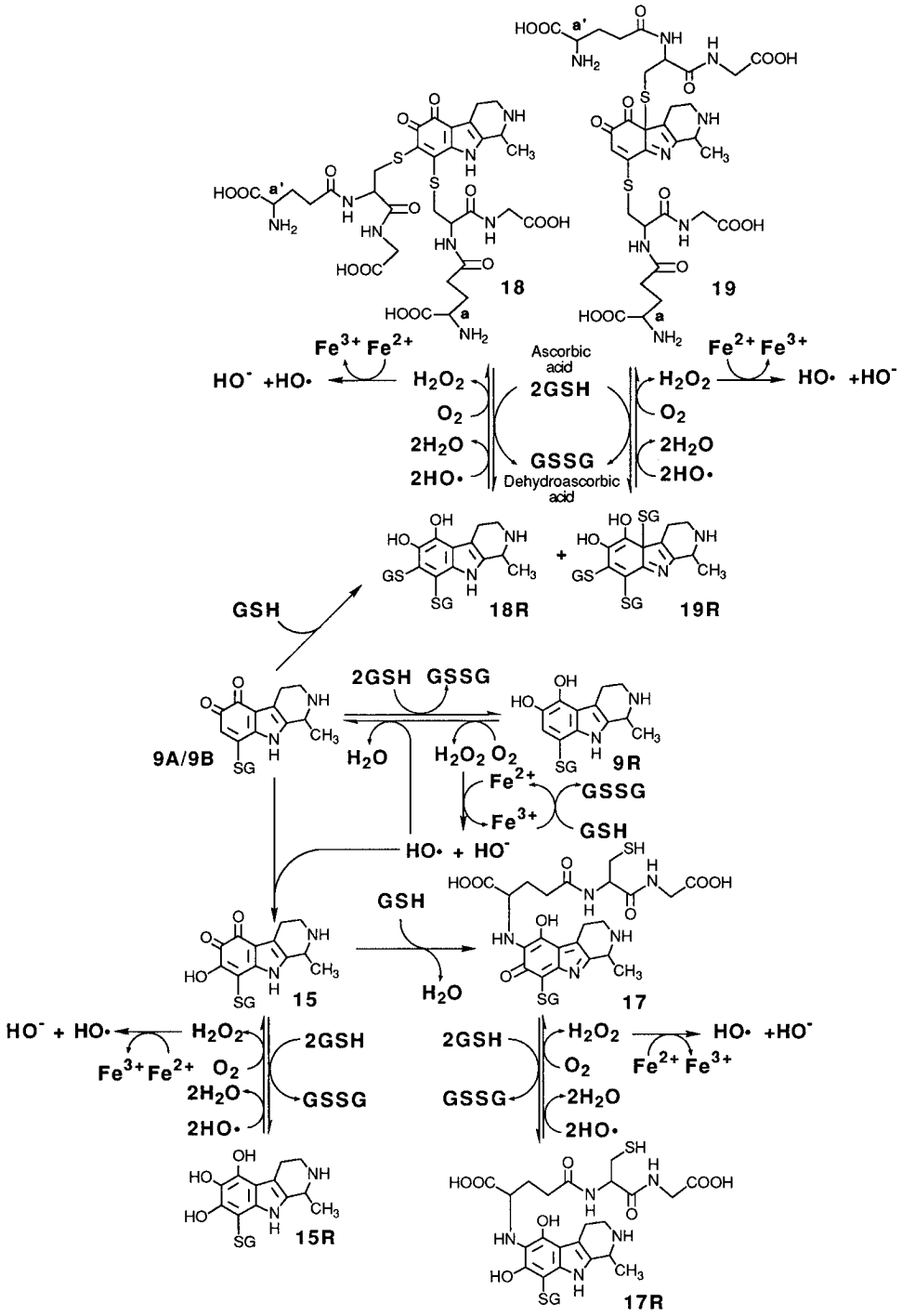

tion of **1** in the cytoplasm of serotonergic neurons would lead to significant and irreversible losses of GSH as a consequence of reactions of the tripeptide with **8** to give **9A**/**9B**, with the latter compounds to give **18** and **19**, and with **15** to give **17**. Both acute and chronic ethanol drinking do indeed evoke significant decreases in brain levels of GSH without corresponding increases in GSSG levels despite the fact that the activities of enzymes associated with biosynthesis of GSH are increased.[33,36]

In summary, metabolism of ethanol in the cytoplasm of serotonergic neurons with resultant generation of acetaldehyde and HO$^{\bullet}$ in the presence of 5-HT and GSH (and other intraneuronal antioxidants/reductants) provide conditions for both the endogenous synthesis of **1**, its oxidation to **8**, and formation of **9**, **15**, and **17**−**19** which in turn would establish several redox cycling systems and elevated fluxes of H_2O_2 and HO$^{\bullet}$. It should be noted that all of the β-carboline adducts formed by addition of GSH to dione **8** in such intraneuronal reactions would be present in diastereomeric forms as was the case in this *in vitro* investigation. Thus, although diastereomers **9A** and **9B** could be separated, the putative *in vivo* redox cycling reactions of all glutathionyl conjugates derived from **8** would necessarily involve diastereomeric mixtures. The redox cycling chemistry of such mixtures were, therefore, of particular interest in this investigation. Reduced oxygen species formed as byproducts of such intraneuronal redox cycling reactions might contribute to oxidative damage[33,44,45] and the profound degeneration of serotonergic pathways that occurs in the brains of alcoholics.[21] Experiments with animals implicate deficiencies of

5-HT[12−15] and loss of certain serotonergic pathways, in the nucleus accumbens for example,[13−15] with increased preference for ethanol drinking.

Experimental Section

5-Hydroxytryptamine hydrochloride (5-HT·HCl), acetaldehyde, L-cysteine (CySH), glutathione (GSH, free base), peroxidase (type VI from horseradish, EC 1.11.1.7), catalase (bovine liver, EC 1.11.1.6), superoxide dismutase (SOD; bovine, suspension in 3.8 M ammonium sulfate solution pH 7.0), β-nicotine adenine dinucleotide phosphate (reduced form, NADPH), ascorbic acid, diethylenetriaminepentaacetic acid (DTPA), and mannitol were obtained from Sigma (St. Louis, MO) and were used without additional purification. Hydrogen peroxide and ferrous ammonium sulfate hexahydrate were obtained from Mallinckrodt (Paris, KY). Ferric chloride hexahydrate and copper sulfate were obtained from Fisher (Springfield, NJ). 1-Methyl-6-hydroxy-1,2,3,4-tetrahydro-β-carboline (**1**) was prepared by condensation of 5-HT with acetaldehyde as described elsewhere.[24]

Cyclic voltammograms were obtained at a pyrolytic graphite electrode (PGE; Pfizer Minerals, Pigments and Metals Division, Easton, PA), having an approximate surface area of 12 mm^2, using a BAS model 100A electrochemical analyzer (Bioanalytical Systems, West Lafeyette, IN). The PGE was resurfaced before recording each voltammogram as described previously.[24] All voltammograms were corrected for *iR* drop. Controlled potential electrolyses employed a Princeton Applied Research Corporation (Princeton, NJ) model 173 potentiostat. The working electrode consisted of several plates of pyrolytic graphite having a total surface area of *ca.* 120 cm^2. These electrodes were suspended into the solution containing the appropriate supporting electrolyte and compound of interest (typically 30 mL) contained in the working electrode compartment of the electrochemical cell. Conventional three-compartment electrochemical cells were employed for voltammetry and controlled potential electrolyses and utilized a platinum gauze counter electrode and a saturated calomel reference electrode (SCE). All controlled potential electrolyses were carried out with the solution in the working electrode compartment stirred with a Teflon-coated magnetic stirring bar and N_2 gas bubbling vigorously through the solution. Before recording each cyclic voltammogram the solution in the working electrode compartment was thoroughly deoxygenated with N_2 gas for at least 3 min. Unless otherwise stated, all potentials are referenced to the SCE at ambient temperature (22 ± 2 °C).

High-performance liquid chromatography (HPLC) employed either a Bio-Rad (Richmond, CA) binary gradient system equipped with dual model 1300 pumps or a Gilson (Middleton, WI) gradient system equipped with dual model 306 pumps (25 mL pump heads), and a Gilson Holochrome detector set at 254 nm. A preparative reversed phase column (J. T. Baker, Phillipsburg, NJ; Bakerbond C_{18}; 25 × 2.1-cm; 10 μm particle size) was employed for all HPLC experiments. Four mobile phase solvents were used. Solvent A was prepared by adding concentrated trifluoroacetic acid (TFA) to deionized water until the pH was 3.0. Solvent B was prepared by adding TFA to 2.0 L of HPLC grade acetonitrile (MeCN) and 2.0 L of deionized water until the measured pH was 3.0. Solvent C was prepared by adding 30 mL of concentrated ammonium hydroxide solution (NH_4OH) to 4.0 L of deionized water; the pH of this solution was then adjusted to 3.0 by addition of TFA. Solvent D was prepared by adding TFA to 1.6 L of MeCN and 2.4 L of deionized water until the measured pH was 3.0.

HPLC method I, used to monitor the course of oxidation reactions of **1** in the presence of GSH and to separate and isolate the products formed in the reaction between **8** and GSH, employed the following mobile phase gradient: 0−2 min, 100% solvent C; 2−15 min, linear gradient to 15% solvent D; 15−25 min, linear gradient to 25% solvent D; 25−40 min, linear gradient to 100% solvent D. The flow rate was constant at 8.0 mL min^{-1}.

HPLC method II, used to separate and isolate the products of electrochemical oxidation of **1** and the products formed upon reaction of **8** with GSH, employed the following gradient system: 0−30 min, linear gradient from 100% solvent A to 100% solvent B; 30−45 min, 100% solvent B. The flow rate was constant at 8.0 mL min^{-1}.

HPLC method III, used to separate and purify diastereomers **9A** and **9B**, and **19A** and **19B** and to desalt compound **18**, employed the following gradient: 0−50 min, linear gradient from 100% solvent A to 60% solvent B; 50−55 min, linear gradient to 100% solvent B. The flow rate was constant at 8.0 mL min^{-1}.

Low- and high-resolution fast atom bombardment mass spectrometry (FAB-MS) was carried out with a VG Instruments (Manchester, UK) ZAB-E spectrometer. ^1H and ^{13}C NMR spectra were recorded on a Varian model XL-300 spectrometer. UV−visible spectra were recorded on a Hewlett-Packard model 8452A diode array spectrophotometer.

Oxygen consumption rates were measured with a Clark-type oxygen electrode system (YSI model 5300, Yellow Springs, OH) equipped with a thermostated micro oxygen chamber (600 μL) and a micro oxygen probe.

The HO•-generating system employed was based on that originally described by Udenfriend et al.[46] The sequence of additions and final concentrations of reagents were as follows: 5.2 mL of pH 7.4 phosphate buffer (μ = 0.2), 1.5 mL of **1** (2.5 μM to 0.25 mM), 1.0 mL of ascorbic acid (1.0 mM), 0.1 mL of Na_2 EDTA (240 μM), 1.0 mL of ferrous ammonium sulfate (200 μM), and 1.2 mL of H_2O_2 (1.0 mM), giving a total volume of 10.0 mL. When GSH was included in the reaction mixture it was dissolved in the 5.2 mL of pH 7.4 phosphate buffer to give the desired concentration in the final 10 mL. Reaction solutions were stirred at ambient temperature (22 ± 2 °C) and were exposed to the atmosphere.

In the sections that follow, the procedures employed to synthesize, isolate, purify, and spectroscopically characterize new compounds are described in detail. While full chemical names are provided for each compound, for simplicity assignments of proton resonances in ^1H NMR spectra employ the atom numbering systems shown in Schemes 2−4. A tabulation of ^1H NMR chemical shift data for GSH, **8**, **9A**, **9B**, **17**, **17R**, **18**, **19A**, and **19B** are provided as Supporting Information.

Synthesis of Diastereomers of 8-*S*-Glutathionyl-1-methyl-1,2,3,4-tetrahydro-β-carboline-5,6-dione (9A and 9B) and Glycine, L-γ-Glutamyl-L-cysteinyl-, 2→1′-Sulfide with *N*-(2,3,4,7-Tetrahydro-5-hydroxy-8-mercapto-1-methyl-7-oxo-1*H*-pyrido[3,4-*b*]indol-6-yl)-L-γ-glutamyl-L-cysteinylglycine (17). In order to prepare sufficient quantities of **9A**, **9B**, and **17** to permit their structure elucidation by spectroscopic methods, 1-methyl-1,2,3,4-tetrahydro-β-carboline-5,6-dione (**8**) was first prepared by controlled potential electrooxidation of **1** at pH 1.5. Compound **1** (1.5 mg) was dissolved in 30 mL of pH 1.5 phosphate buffer (μ = 0.2) and electrooxidized at 1.0 V for 20 min at which time ≥95% of **1** was oxidized to **8**. The entire volume of the bright purple solution was then introduced onto the preparative reversed phase HPLC column by pumping through one of the HPLC pumps and the reaction products were separated using method II; **8** eluted at t_R = 24 min. The mobile phase (*ca.* 10 mL) containing **8** (*ca.* 0.7 mM) was collected, and to it was added GSH (15 mg; *ca.* 5 mM). The resulting solution (pH 3.0) was stirred for approximately 30 min at ambient temperature during which time the initially bright purple color of **8** faded to give a colorless solution. The entire product solution was then introduced onto the preparative HPLC column, and the components were separated using method II. Two major chromatographic peaks eluted at t_R = 20 min (**17R**) and 24 min (**9R**). The eluents corresponding to these peaks were collected separately and freeze-dried. The $E^{o\prime}$ values for the **9A**/**9B**/**9R** and **17**/**17R** couples at pH 3.0 and 7.4 are −35 and −220 mV, and 36 and −148 mV, respectively. Thus, at pH 3 both **9A**/**9B** and **17** are more easily reducible than at pH 7.4. Conversely, **9R** and **17R** are more difficult to oxidize at pH 3 than at pH 7.4. It is for these reasons that under the conditions employed above **9R** and **17R** represent the major reaction products. However, prolonged exposure of the colorless product solution to the atmosphere resulted in the development of a purple/blue color due to formation of **9A**/**9B** and **17**. The solid sample of **9R** was dissolved in 10 mL of pH 3.0 phosphate buffer (μ = 0.2) and oxidized by controlled

potential electrolysis at 200 mV for approximately 10 min. Aliquots (2.0 mL) of the bright purple product solution were then injected into the HPLC system (method III), and the eluents containing **9A** (t_R = 32.5 min) and **9B** (t_R = 33.0 min) were collected separately and freeze-dried.

The solid sample of **17R** was dissolved in 10 mL of pH 3.0 phosphate buffer and oxidized by controlled potential electrolysis at 200 mV for approximately 20 min. The resulting blue product solution was injected into the HPLC system (method II), and the single product that eluted at t_R = 21.0 min (**17**) was collected and freeze-dried. The above procedures were repeated numerous times in order to obtain sufficient quantities of **9A**, **9B**, **17R**, and **17**.

5,5-Bi(1-methyl-6-hydroxy-1,2,3,4-tetrahydro-β-carboline) (7), 1-Methyl-1,2,3,4-tetrahydro-β-carboline-5,6-dione (8), and 5-*S*-Glutathionyl-1-methyl-6-hydroxy-1,2,3,4-tetrahydro-β-carboline (10). The synthesis and spectroscopic evidence for the structures of **7**, **8**, and **10** have been described in detail elsewhere.[24]

8-*S*-Glutathionyl-1-methyl-1,2,3,4-tetrahdyro-β-carboline-5,6-diones (9A and 9B). Compounds **9A** and **9B** were isolated as purple solids. In pH 7.4 phosphate buffer (μ = 1.0) these compounds exhibited UV−visible spectra with λ_{max}, nm (log ϵ_{max}, M^{-1} cm^{-1}) as follows: **9A**, 552 (3.17), 370 sh (3.83), 346 (3.91), 248 (4.20); **9B**, 548 (3.23), 370 sh (3.83), 346 (3.91), 248 (4.20). FAB-MS (3-nitrobenzyl alcohol matrix) of **9A** gave *m*/*e* = 522.1629 (MH^+, 50%, $C_{22}H_{28}N_5O_8S$; calcd *m*/*e* = 522.1659) and *m*/*e* = 524.1848 ($MH_2{\cdot}H^+$, 95%, $C_{22}H_{30}N_5O_8S$; calcd *m*/*e* = 524.1815). FAB-MS (thioglycerol/glycerol matrix) on **9B** gave *m*/*e* = 522.1665 (MH^+, 50%, $C_{22}H_{28}N_5O_8S$; calcd *m*/*e* = 522.1659) and *m*/*e* = 524.1831 ($MH_2{\cdot}H^+$, 90%, $C_{22}H_{30}N_5O_8S$; calcd *m*/*e* = 524.1815). Thus, **9A** and **9B** both had a molar mass of 521 g and an elemental formula $C_{22}H_{27}N_5O_8S$ and, hence, consisted of one residue each of dione **8** and GSH. The ease of reduction of both **9A** and **9B** accounts for the appearance of intense pseudomolecular ions of their reduced forms, *i.e.* $MH_2{\cdot}H^+$, in FAB-MS. ^{1}H NMR (D_2O) of **9A** gave δ 5.89 (s, 1H, C(7)-H), 4.83−4.81 (m, 1H, C(d)-H), 4.58−4.57 (m, 1H, C(1)-H), 3.88 (s, 2H, C(f)-H_2), 3.72 (t, *J* = 6.3 Hz, 1H, C(a)-H), 3.59−3.54 (m, 2H, C(3)-H, C(e)-H), 3.38−3.34 (m, 2H, C(3)-H, C(e)-H), 2.88 (s, 2H, C(4)-H_2), 2.47 (t, *J* = 7.5 Hz, C(c)-H_2), 2.08 (q, *J* = 7.2 Hz, 2H, C(b)-H_2), 1.63 (d, *J* = 6.6 Hz, 3H, C(1)-CH_3). ^{1}H NMR (D_2O) of **9B** gave δ 5.95 (s, 1H, C(7)-H), 4.82 (m, 1H, C(d)-H), 4.60 (q, *J* = 6.6 Hz, 1H, C(1)-H), 3.76 (s, 2H, C(f)-H_2), 3.70 (t, *J* = 6.3 Hz, 1H, C(a)-H), 3.61−3.53 (m, 2H, C(3)-H, C(e)-H), 3.39−3.35 (m, 2H, C(3)-H, C(e)-H), 2.91 (m, 2H, C(4)-H_2), 2.47 (t, *J* = 7.5 Hz, 2H, C(c)-H_2) 2.06 (q, *J* = 6.6 Hz, 2H, C(b)-H_2), 1.64 (d, *J* = 6.6 Hz, 3H, C(1)-CH_3). The above assignments were based on comparisons of the spectra of **9A** and **9B** with those of **8** and GSH and by use of two-dimensional (2D) correlated spectroscopy (COSY) experiments. The ^{1}H NMR spectrum of **8** in D_2O exhibited two doublets (*J* = 10.2 Hz) at δ 7.29 (C(8)-H) and 6.01 (C(7)-H).[24] The upfield location of the latter resonance is expected because of the adjacent carbonyl group at C(6); similar upfield shifts have been reported for the α proton of several structurally-related *o*-diketones such as tryptamine-4,5-dione[47,48] and 1,2-naphthoquinone.[49] The expected 1,4-Michael addition of GSH to **8** was indicated by the loss of the low-field C(8)-H resonance to give, ultimately, **9A** and **9B** that retain high-field (singlet) resonances at δ 5.89 and 5.95, respectively. Unequivocal proof of the structures of **8** and **9** could, in principle, be obtained from the COSY spectrum of **9R** in a nonexchanging solvent which should show a cross peak between H-7 and C(6) phenol proton. However, the very great ease of autoxidation of **9R** to **9A**/**9B** and the fact that none of these compounds were soluble in nonexchanging solvents such as dimethyl sulfoxide or acetonitrile precluded such ^{1}H NMR experiments. Attempts to obtain ^{13}C NMR spectra of **9A** and **9B** were unsuccessful owing to the tendency of these compounds to polymerize/decompose to a dark purple gel when present in high concentration in solution for the prolonged periods of time necessary for such experiments. Nevertheless, the spectroscopic properties of **9A** and **9B** were clearly almost identical, indicating that these compounds are diastereomers. Anal. ($C_{22}H_{27}N_5O_8S{\cdot}2CF_3COOH$). Calcd: C, 41.66; H, 3.87; N, 9.35; S, 4.27. Found: C, 41.51; H, 3.99; N, 9.17; S, 4.44. Combustion analysis was carried out on a equimolar mixture of diastereomers.

Glycine, L-γ-glutamyl-L-cysteinyl-, 2→1′-Sulfide with *N*-(2,3,4,7-Tetrahydro-5-hydroxy-8-mercapto-1-methyl-7-oxo-1*H*-pyrido[3,4-*b*]indol-6-yl)-L-γ-glutamyl-L-cysteinylglycine (17). Compound **17** was isolated as a deep blue solid, mp = 185−190 °C dec. In pH 7.4 phosphate buffer **17** exhibited a UV−visible spectrum with λ_{max}, nm (log ϵ_{max}, M^{-1} cm^{-1}) at 598 (3.39), 348 (3.79), and 270 (4.22). FAB-MS (thioglycerol/glycerol matrix) gave *m*/*e* 829.2562 ($MH_2{\cdot}H^+$, 5%, $C_{32}H_{45}N_8O_{14}S_2$; calcd *m*/*e* = 829.2497). The ease of reduction of **17** accounts for the appearance of the $MH_2{\cdot}H^+$ pseudomolecular ion of this compound. ^{1}H NMR (D_2O) gave δ 4.32−4.30 (m, 2H, C(d)-H, C(d′)-H), 3.89 (s, 2H, C(f)-H_2), 3.76 (t, *J* = 6.0 Hz, 1H, C(a)-H), 3.71−3.64 (m, 2H, C(3)-H_2), 3.68 (s, 2H, C(f)-H_2) 3.53−3.41 (m, 3H, C(a′)-H, C(e)-H_2), 3.32 (d, *J* = 6.0 Hz, 2H, C(e′)-H_2), 3.22 (m, 2H, C(4)-H_2), 2.50−2.49 (m, 2H, C(c)-H_2), 2.34 (t, *J* = 4.5 Hz, 2H, C(c′)-H_2), 2.19 (q, *J* = 7.2 Hz, 2H, C(b)-H_2), 1.96−1.92 (m, 2H, C(b′)-H_2), 1.70 (d, *J* = 6.6 Hz, 3H, C(1)-CH_3). 2D COSY experiments were in accord with the above ^{1}H NMR assignments and also revealed that the resonance at δ 1.70 (d, C(1)-CH_3) was coupled to a resonance at δ 4.70 (C(1)-H) which was masked by a large solvent (HOD) peak in the one-dimensional spectrum. ^{13}C NMR (D_2O) showed nine resonances corresponding to carbonyl carbons at δ 181.14, 177.40, 177.29, 177.18, 177.03, 176.48, 176.35, 174.25, and 173.76; seven aromatic carbon resonances at δ 149.61, 141.31, 136.25, 133.45, 132.86, 121.86, and 120.05; and 16 aliphatic carbon resonances at δ 56.82, 56.25, 56.11, 55.92, 50.85, 41.96, 41.83, 39.77, 39.69, 39.64, 37.22, 34.28, 34.15, 28.82, 22.05 and 19.61. Anal. ($C_{32}H_{42}N_8O_{14}S_2{\cdot}2CF_3COOH{\cdot}2H_2O$). Calcd: C, 39.63; H, 4.40; N, 10.27; S, 5.87. Found: C, 39.37; H, 4.62; N, 10.44; S, 4.62. Experimental evidence indicates that **9A**/**9B** are attacked by $HO^{\bullet}$ to give **15** that subsequently reacts with excess free GSH to give **17** (Figures 6, 7, and 9 and related discussion). The absence of a resonance corresponding to H-7 in the ^{1}H NMR spectrum of **17** and the fact that the C(1)-H, C(3)-H_2, and C(4)-H_2 resonances remain supports the conclusion that **15** and **17** contain a hydroxyl substituent at C(7). The mass spectrum, ^{1}H NMR spectrum, and elemental analysis data for the diastereomers of **17** support structures in which the Schiff base residue could be linked at C(5), C(6), or C(7). However, linkage of the Schiff base residue at either the C(5) or C(7) position would result in structures that contain ten carbonyl groups. By contrast, linkage at the C(6) position would give a structure containing only nine carbonyl residues in accord with that observed in the ^{13}C NMR spectrum of **17**. The significant differences between the UV−visible spectra of **17** and **9A**/**9B** are also in accord with the structure proposed for **17**.

Glycine, L-γ-Glutamyl-L-cysteinyl-, 2→1′-Sulfide with *N*-(2,3,4,9-Tetrahydro-5,7-dihydroxy-8-mercapto-1-methyl-1*H*-pyrido[3,4-*b*]indol-6-yl)-L-γ-glutamyl-L-cysteinylglycine (17R). In order to prepare **17R** in quantities suitable for spectroscopic structure elucidation and as a reference compound, a solution of dione **8** (0.22 mM, 30 mL dissolved in the HPLC method II mobile phase, pH 3.0) was first prepared by controlled potential electrooxidation of **1** as described previously. The pH of this solution was adjusted to 6.0 by careful addition of 10% aqueous NH_4OH. GSH (100 mg, 10.8 mM) was then added, and the resulting solution was stirred for 4 h. HPLC (method II) revealed that one major product (**17R**) was formed under these conditions (t_R = 20 min). The compound eluted under this peak was collected and freeze-dried to give a white solid (**17R**). The UV spectrum of this compound dissolved in pH 3.0 phosphate buffer showed λ_{max}, nm (log λ_{max}, M^{-1} cm^{-1}) at 334 (4.02), 300 (4.18) and 262 sh (4.47). A cyclic voltammogram (ν = 200 mV s^{-1}) of **17R** (0.2 mM) at pH 3.0 exhibited a single oxidation peak (E_p = 60 mV) on the initial anodic sweep. After scan reversal a quasi-reversible reduction peak appeared (E_p = 12 mV). This cyclic voltammogram was identical to that of **17** under the same experimental conditions. Compound **17R** was very easily autoxidized to **17** in solution at pH 7.4 (see earlier discussion). FAB-MS (thioglycerol/glycerol matrix) of **17R** gave *m*/*e* = 829.2526 (MH^+, 9%, $C_{32}H_{45}N_8O_{14}S_2$; calcd *m*/*e* = 829.2497). ^{1}H NMR (D_2O) gave 4.78 (q, *J* = 6.9 Hz, 1H, C(1)-H), 4.35 (t,

J = 6.0 Hz, 2H, C(d)-H, C(d′)-H), 3.76 (t, J = 6.0 Hz, 1H, C(a)-H), 3.70 (s, 4H, C(f)-H_2, C(f′)-H_2), 3.64 (t, J = 6.3 Hz, 1H, C(a′)-H), 3.49−3.47 (m, 1H, C(e)-H), 3.30 (m, 4H, C(3)-H_2, C(e)-H), C(e′)-H), 3.24 (m, 3H, C(4)-H_2, C(e′)-H), 2.35−2.16 (m, 4H, C(c)-H_2, C(c′)-H_2), 1.98 (m, 4H, C(b′)-H_2, C(b)-H_2), 1.71 (d, J = 6.6 Hz, 3H, C(1)-CH_3).

7,8-Bi(*S*-glutathionyl-1-methyl-1,2,3,4-tetrahydro-*β*-carboline-5,6-dione) (18). In order to optimize formation of this compound, GSH (9.0 mg, *ca.* 1.0 mM) was added to a 0.22 mM solution (30 mL) of **8** dissolved in the mobile phase (pH 3.0) of HPLC method II and the resulting solution stirred for 2 h. The pH of the solution was then adjusted to 7.4 ± 0.1 with pH 7.4 phosphate buffer (μ = 1.0), and 50 mg of GSH was added. The solution was then stirred at room temperature for 8 h. The entire solution was then pumped onto the preparative reversed phase HPLC column, and the components were separated using method I. Compound **18** eluted under the chromatographic peak at t_R = 40 min. The eluent containing **18** was collected and desalted using HPLC method III (t_R = 42 min). The desalted solution of **18** was then freeze-dried to give a purple solid. In pH 7.4 phosphate buffer **18** exhibited a UV−visible spectrum with λ_{max}, nm (log ϵ_{max}, M^{-1} cm^{-1}) at 536 (3.44), 3.64 sh (3.79), 308 (4.15), 246 sh (4.35). FAB-MS (thioglycerol/glycerol/TFA matrix) gave m/e = 827.2319 (MH^+, 9%, $C_{32}H_{43}N_8O_{14}S_2$; calcd m/e = 827.2340). Thus, **18** had a molar mass of 826 g and a molecular formula $C_{32}H_{42}N_8O_{14}S_2$. ^{1}H NMR (D_2O) gave δ 4.77−4.67 (m, 3H, C(1)-H, C(d)-H, C(d′)-H), 4.09 (t, J = 6.3 Hz, 1H, C(a)-H), 4.00 (s, 2H, C(f)-H_2), 3.94 (s, 2H, C(f′)-H_2), 3.89 (t, J = 6.3 Hz, 1H, C(a′)-H), 3.73−3.67 (m, 1H, C(3)-H), 3.49−3.45 (m, 1H, C(3)-H), 3.29−3.18 (m, 2H, C(e)-H, C(e′)-H), 3.08 (bs, 2H, C(4)-H_2), 3.03−2.95 (m, 2H, C(e)-H, C(e′)-H), 2.56 (t, J = 6.3 Hz, 4H, C(c)-H_2, C(c′)-H_2), 2.25−2.17 (m, 4H, C(b)-H_2, C(b′)-H_2), 1.71 (d, J = 6.9 Hz, 3H, C(1)-CH_3). Compound **18** has the same molecular weight and elemental composition as **17**, and both compounds have similar ^{1}H NMR spectra. However, as discussed previously, **17** is formed via **15** as a result of $HO^•$ attack on **9A/9B** whereas **18** is formed as a more minor product by attack of GSH on **9A/9B** (Figure 9 and related discussion). Furthermore, the UV−visible spectrum of purple **18** at pH 7.4 is quite different to that of blue **17** but quite similar to that of purple **9A/9B** which differ from **18** only by the absence of a glutathionyl residue at C(7). Additionally, the cyclic voltammogram of **17** is quite different to that of both **9A/9B** and **18**, the latter compounds all exhibiting a single reversible couple. The shift of $E^{\circ\prime}$ for the **18/18R** couple to somewhat more negative potentials than that for the **9A/9B/9R** couples is in accord with the electron-releasing effects of the second glutathionyl residue at C(7).

4,8-Bi(*S*-glutathionyl-1-methyl-1,2,3,4-tetrahydro-*β*-carboline-5,6-dione) (19A and 19B). In order to optimize the synthesis of **19A** and **19B**, 9.0 mg of GSH (*ca.* 1.0 mM) was added to a 0.22 mM solution of dione **8** (30 mL in HPLC method II mobile phase, pH 3.0) and stirred at room temperature for 2 h. The pH of the solution was then adjusted to 10.3 ± 0.1 by addition of 20% NH_4OH. GSH (60 mg) was added to the resulting solution which was then stirred for 1 h. Following filtration (0.45 μm, type HA filter, Millipore, Bedford, MA) the entire solution was pumped onto the reversed phase HPLC column, and the components were separated using method I. Compounds **19A** and **19B** coeluted at t_R = 44 min. After freeze-drying the eluent containing **19A** and **19B** the resulting orange solid was dissolved in 10 mL of deionized water and separated and desalted using HPLC method III using repetitive 2.0 mL injections. Compound **19A** eluted at t_R = 50.0 min and **19B** at t_R = 50.5 min. The orange solutions eluted under each of these peaks were collected separately and freeze-dried to give orange solids. In pH 7.4 phosphate buffer **19A** exhibited a UV−visible spectrum with λ_{max}, nm (log ϵ_{max}, M^{-1} cm^{-1}) at 514 (3.62), 384 (4.30), 262 sh (4.17). FAB-MS (thioglycerol/TFA matrix) gave m/e = 827.2370 (MH^+, 3%, $C_{32}H_{43}N_8O_{14}S_2$; calcd m/e = 827.2340). ^{1}H NMR (D_2O) gave δ 6.67 (s, 1H, C(7)-H), 4.95 (q, J = 5.1 Hz, 1H, C(1)-H), 4.71 (t, J = 6.6 Hz, 2H, C(d)-H, C(d′)-H), 4.03 (s, 2H, C(f)-H_2), 3.88 (s, 2H, C(f′)-H_2), 3.83−3.75 (m, 2H, C(a)-H, C(a′)-H), 3.71−3.65 (m, 2H, C(3)-H, C(e)-H), 3.54−3.45 (m, 3H, C(3)-H, C(e)-H, C(e′)-H), 3.37−3.30 (m, 1H, C(e′)-H), 3.13 (m, 2H, C(4)-H_2), 2.54 (t, J = 7.2 Hz, 2H, C(c)-H_2), 2.48−2.36 (m, 2H, C(c′)-H_2), 2.17−2.03 (m, 4H, C(b)-H_2, C(b′)-H_2), 1.72 (d, J = 6.6 Hz, 3H, C(1)-CH_3). ^{13}C NMR (D_2O) showed 10 carbonyl carbon resonances at δ 177.89, 177.40, 177.30, 177.08, 175.88, 175.36, 175.18, 174.51, 173.95, and 154.33; 6 aromatic carbon resonances at δ 141.92, 131.16, 128.41, 127.20, 118.81, and 118.14; and 16 aliphatic carbon resonances at δ 56.39, 56.20, 56.02, 55.89, 55.75, 55.62, 55.49, 51.19, 47.14, 44.14, 42.69, 36.65, 33.97, 28.62, 22.14, and 19.69.

In pH 7.4 phosphate buffer **19B** exhibited a UV−visible spectrum with λ_{max}, nm (log ϵ_{max}, M^{-1} cm^{-1}) at 512 (3.61), 382 (4.30), 260 sh (4.18). FAB-MS (glycerol/TFA matrix) gave m/e = 827.2327 (MH^+, 22%, $C_{32}H_{43}N_8O_{14}S_2$; calcd m/e = 827.2340). ^{1}H NMR (D_2O) gave δ 6.62 (s, 1H, C(7)-H), 4.93 (q, J = 5.1 Hz, 1H, C(1)-H), 4.69 (t, J = 5.7 Hz, 2H, C(d)-H, C(d′)-H), 4.02 (s, 2H, C(f)-H_2), 3.85 (s, 2H, C(f′)-H_2), 3.82−3.75 (m, 2H, C(a)-H, C(a′)-H), 3.69−3.63 (m, 2H, C(3)-H, C(e)-H), 3.51−3.42 (m, 3H, C(3)-H, C(e)-H, C(e′)-H), 3.39−3.29 (m, 1H, C(e′)-H), 3.11 (m, 2H, C(4)-H_2), 2.53 (t, J = 7.2 Hz, 2H, C(c)-H_2), 2.45−2.36 (m, 2H, C(c′)-H_2), 2.16−2.05 (m, 4H, C(b′)-H_2, C(b)-H_2), 1.71 (d, J = 6.6 Hz, 3H, C(1)-CH_3). ^{13}C NMR (D_2O) of **19B** showed 10 carbonyl carbon resonances at δ 172.66, 172.49, 171.31, 171.16, 171.08, 171.03, 170.46, 169.85, and 149.61; 6 aromatic carbon resonances at δ 137.19, 126.52, 123.49, 122.53, 114.17, and 113.48; and 16 aliphatic carbon resonances at δ 51.64, 51.59, 51.52, 51.03, 50.92, 46.47, 42.55, 39.63, 39.60, 39.49, 37.87, 32.20, 29.34, 23.97, 17.55, and 15.20. The mass spectral data obtained for the compounds designated **19A** and **19B** (molar mass 826 g, molecular formula $C_{32}H_{42}N_8O_{14}S_2$) indicate that they consist of one residue of dione **8** and two residues of GSH. These isomers are formed by the reaction of GSH with diastereomers **9A/9B**. Furthermore, the ^{1}H NMR spectra of **19A** and **19B** reveal that the C(7)-H, C(3)-H_2, and C(4)-H_2 resonances are present. Accordingly, it can be concluded that the glutathionyl residue that adds to **9A/9B** to give **19A/19B** is linked at the C(4a) and/or C(4b) bridgehead position. The fact that the UV−visible spectra and cyclic voltammetric behaviors of **19A** and **19B** are the same suggests that GSH residue is located at the same bridgehead carbon in all of the isomers. However, the spectral information available on **19A** and **19B**, which must consist of a total of four isomers, does not permit an unequivocal assignment of the linkage site for the bridgehead glutathionyl residue. Thus, the structure presented for **19** in Scheme 4 must be considered to be a tentative assignment at this time.

Acknowledgment. This work was supported in part by funds provided by the Oklahoma Center for the Advancement of Science and Technology (OCAST) through contract No. 4186. Additional support was provided by the PI Research Investment Program, the Vice President for Research, and the Research Council at the University of Oklahoma.

Supporting Information Available: Tabulation of ^{1}H NMR chemical shift data for compounds **8**, **9A**, **9B**, **17**, **17R**, **18**, **19A**, **19B**, and GSH (1 page). Ordering information is given on any current masthead page.

References

(1) Matsubara, K.; Fukishima, S.; Fukui, Y. A. Systematic Regional Study of Brain Salsolinol Levels During and Immediately Following Chronic Ethanol Ingestion in Rats. *Brain Res.* **1987**, *413*, 336−343.

(2) Sjöquist, B. J.; Johnson, H. A.; Borg. S. The Influence of Ethanol on the Catecholamine System in Man as Reflected in Cerebrospinal Fluid and Urine. A New Condensation Product, 1-Carboxysalsolinol. *Drug Alcohol Depend.* **1985**, *16*, 241−249.

(3) Cashaw, J. L.; Geraghty, C. A.; McLaughlin, B. R.; Davis, V. E. Effect of Acute Ethanol Administration on Brain Levels of Tetrahydropapaveroline in *L*-DOPA-Treated Rats. *J. Neurosci. Res.* **1987**, *18*, 497−503.

(4) Beck, O.; Taylor, A.; Faull, K. Serotonin Condensation Product 5-Hydroxymethtryptoline: Evidence for *In Vivo* Formation from Acetaldehyde During Intoxication Using Deuterium-Labeled Ethanol. *Alcohol Alcoholism Suppl.* **1987**, *1*, 743−747.

(5) Melchior, C. L.; Myers, R. D. Preference for Alcohol Evoked by Tetrahydropapaveroline (THP) Chronically Infused in the Cerebral Ventricle of the Rat. *Pharmacol. Biochem. Behav.* **1977**, *7*, 19−35.

(6) Tuomisto, L.; Airaksinen, M. M.; Peura, P.; Eriksson, C. J. P. Alcohol Drinking in the Rat: Increase Following Intracerebroventricular Treatment with Tetrahydro-β-Carbolines. *Pharmacol. Biochem. Behav.* **1982**, *17*, 831−836.
(7) Myers, R. D.; Privette, T. H. A Neuroanatomical Substrate for Alcohol Drinking: Identification of Tetrahydropapaveroline (THP) - Reactive Sites in the Rat Brain. *Brain Res. Bull.* **1989**, *22*, 899−911.
(8) Huttunen, P.; Myers, R. D. Anatomical Localization in Hippocampus of Tetrahydro-β-Carboline-Induced Ethanol Drinking in the Rat. *Alcohol* **1987**, *4*, 181−187.
(9) Davis, V. E.; Walsh, J. M. Alcohol, Amines and Alkaloids: A Possible Biochemical Basis for Alcohol Addiction. *Science* **1970**, *167*, 1005−1007.
(10) Cohen, G.; Collins, M. A. Alkaloids from Catecholamines in Adrenal Tissue: Possible Role in Alcoholism. *Science* **1970**, *167*, 1749−1751.
(11) Myers, R. D.; Evans, J.; Yaksh, T. Ethanol Preference in the Rat: Interactions Between Brain Serotonin and Ethanol, Acetaldehyde, Paraldehyde, 5-HTPP and 5-HTOL. *Neuropharmacology* **1972**, *11*, 539−549.
(12) Melchior, C. L.; Myers, R. D. Genetic Differences in Ethanol Drinking of the Rat Following Injection of 6-OHDA or 5,7-DHT into the Cerebral Ventricles. *Pharmacol. Biochem. Behav.* **1976**, *5*, 63−72.
(13) Myers, R. D.; Quarfordt, S. D. Alcohol Drinking Attenuated by Sertraline in Rats with 6-OHDA or 5,7-DHT lesions in the N. Accumbens: A Caloric Response? *Pharmacol. Biochem. Behav.* **1991**, *40*, 923−928.
(14) McBride, W.; Murphy, J.; Lumeng, L.; Li, T.-K. Serotonin and Ethanol Preference. In: *Recent Developments in Alcoholism*, Galanter, M., Ed.; Plenum Press: New York, 1989; Vol. 7, pp 187−209.
(15) Zhou, F.; Bledsoe, S.; Lumeng, L.; Li, T.-K. Immunostained Serotonergic Fibers are Decreased in Selected Brain Regions of Alcohol-Preferring Rats. *Alcohol* **1991**, *8*, 425−431.
(16) Quarfordt, S.; Kalmus, G.; Myers, R. D. Ethanol Drinking Following 6-OHDA Lesions of Nucleus Accumbens and Tuberculum Olfactorium of the Rat. *Alcohol* **1991**, *8*, 211−217.
(17) McBride, W. J.; Murphy, J. M.; Lumeng, L.; Li, T.-K. Serotonin, Dopamine and GABA Involvement in Alcohol Drinking of Selectively Bred Rats. *Alcohol* **1990**, *7*, 199−205.
(18) Riley, J. N.; Walker, D. W. Morphological Alterations in Hippocampus After Long-Term Alcohol Consumption in Mice. *Science* **1978**, *201*, 646−648.
(19) Walker, D. W.; Hunter, B. E.; Barnes, D. E.; Riley, J. N. An Animal Model of Alcohol-Induced Brain Damage: A Behavioral and Anatomical Analysis. In *Cerebral Defecits in Alcoholism*; Wilkinson, D. A., Ed.: Addiction Research Foundation: Toronto, 1980; pp 123−147.
(20) Harper, C.; Kril, J.; Daly, J. Are We Drinking Our Neurons Away? *Br. Med. J.* **1987**, *294*, 534−536.
(21) Carlsson, A.; Adolfsson, R.; Aquilonius, S.-M.; Gottfries, C.-G.; Oreland, L.; Svennerholm, L.; Winblad, B. Biogenic Amines in Human Brain in Normal Aging, Senile Dementia, and Chronic Alcoholism. In: *Ergot Compounds and Brain Function: Neuroendocrine and Neuropsychiatric Aspects*; Goldstein, M., Ed.; Raven Press: New York, 1980; pp 295−304.
(22) Melchior, C. L.; Deitrich, R. A. Half-Lives and Actions of Intracerebrally Injected Isoquinolines. In *Biological Effects of Alcohol*; Begleiter, Ed.; Plenum Press: New York, 1980; pp 121−129.
(23) Fa. Z.; Dryhurst, G. Interactions of Salsolinol with Oxidative Enzymes. *Biochem. Pharmacol.* **1991**, *42*, 2209−2219.
(24) Zhang, F.; Goyal, R. N.; Blank, C. L.; Dryhurst, G. Oxidation Chemistry and Biochemistry of the Central Mammalian Alkaloid 1-Methyl-6-Hydroxy-1,2,3,4-Tetrahydro-β-Carboline. *J. Med. Chem.* **1992**, *35*, 82−93.
(25) Fa, Z.; Dryhurst, G. Electrochemical and Enzyme-Mediated Oxidations of Tetrahydropapaveroline. *J. Org. Chem.* **1991**, *56*, 7113−7121.
(26) Le, A. D.; Poulos, C. X.; Zuan, B.; Chow, S. The Effects of Selective Blockade of Delta and Mu Opiate Receptors on Ethanol Conusmption by C57BL/6 Mice in a Restricted Access Paradigm. *Brain Res.* **1993**, *630*, 330−332.
(27) Kornet, M.; Goosen, C.; Van Ree, J. M. Opioid Modulation of Alcohol Intake in Monkeys by Low Doses of Naltrexone and Morphine. *Ann. N. Y. Acad. Sci.* **1992**, *654*, 469−471.
(28) Critcher, E. C.; Lin, C. I.; Patel, J.; Myers, R. D. Attenuation of Alcohol Drinking in Tetrahydroisoquinoline-Treated Rates by Morphine and Naltrexone. *Pharmacol. Biochem. Behav.* **1983**, *18*, 225−229.
(29) O'Brien, C. P. Treatment of Alcoholism as a Chronic Disorder. *Alcohol* **1994**, *11*, 433−437.
(30) Froehlich, J. C.; Zqeifel, M.; Harts, J.; Lumeng, L. and Li, T.-K. Importance of Delta Opioid Receptors in Maintaining High Alcohol Drinking. *Psychopharmacology* **1991**, *103*, 467−472.
(31) Aragon, C. M.; Rogan, F.; Amit, Z. Ethanol Metabolism in Rat Brain Homogenates by a Catalase-H_2O_2 System. *Biochem. Pharmacol.* **1992**, *44*, 93−98.
(32) Hansson, T.; Tindberg, N.; Ingelman-Sundberg, M.; Köhler, C. Regional Distribution of Ethanol-Inducible Cytochrome P450 IIE1 in the Rat Central Nervous System. *Neuroscience* **1990**, *34*, 451−463.
(33) Montoliu, C.; Vallés, S.; Renau-Piqueras, J.; Guerri, C. Ethanol-Induced Oxygen Radical Formation and Lipid Peroxidation in Rat Brain: Effect of Chronic Alcohol Consumption. *J. Neurochem.* **1994**, *63*, 1855−1862.
(34) Persson, J. O.; Terelius, Y.; Ingelman-Sundberg, M. Cytochrome P450-Dependent Formation of Oxygen Radicals. Isoenzyme-Specific Inhibition of P450-Mediated Reduction of Oxygen and Carbon Tetrachloride. *Xenobiotica* **1990**, *20*, 887−890.
(35) Ingelman-Sundberg, M.; Johansson, I. Mechanisms of Hydroxyl-Radical Formation of Ethanol Oxidation By Ethanol-Inducible and Other Forms of Rabbit Liver Microsomal Cytochrome P450. *J. Biol. Chem.* **1984**, *259*, 6447−6458.
(36) Guerri, C.; Grisolía, S. Changes in Glutathione in Acute and Chronic Alcohol Intoxication. *Pharmacol. Biochem. Behav. Suppl.* **1980**, *13*, 53−61.
(37) Beck, O.; Bosin, T. R.; Lundman, A.; Borg, S. Identification and Measurement of 6-Hydroxy-1-Methyl-1,2,3,4-Tetrahydro-β-Carboline by Gas Chromatography - Mass Spectrometry. *Biochem. Pharmacol.* **1982**, *31*, 2517−2521.
(38) Beck, O.; Faull, K. F.; Barchas, J. D.; Johnson, J. V.; Yost, R. A. Chiral Analysis of Urinary 5-Hydroxymethtryptoline: Implications for Endogenous Biosynthesis and Formation During Ethanol Intoxication. In *Aldehyde Adducts in Alcoholism*; Collins, M. A., Ed.; Alan R. Liss, Inc.: New York, 1985; pp 145−160.
(39) Slivka, A.; Mytilineou, C.; Cohen, G. Histochemical Evaluation of Glutathione in Brain. *Brain Res.* **1987**, *409*, 275−284.
(40) Frank, D. M.; Arora, P. K.; Blumer, J. L.; Sayre, L. M. Model Study of the Bioreduction of Paraquat, MPP^+, and Analogs. Evidence Against a "Redox Cycling" Mechanism in MPTP Neurotoxicity. *Biochem. Biophys. Res. Commun.* **1987**, *147*, 1095−1104.
(41) Richter, H. W.; Waddell, W. H. Oxidation of Dopamine by Hydroxyl Radical in Aqueous Solution. *J. Am. Chem. Soc.* **1983**, *105*, 5435−5440.
(42) Wrona, M. Z.; Yang, Z.; McAdams, M.; O'Connor-Coates, S.; Dryhurst, G. Hydroxyl Radical-Mediated Oxidation of Serotonin: Potential Insights into the Neurotoxicity of Methamphetamine. *J. Neurochem.* **1995**, *64*, 1390−1400.
(43) Halliwell, B. Reactive Oxygen Species and the Central Nervous System. *J. Neurochem.* **1992**, *59*, 1609−1623.
(44) Rouach, H.; Ribiere, C.; Park, M. K.; Saffar, C.; Nordmann, R. Lipid Peroxidation and Brain Mitochondrial Damage Induced by Ethanol. *Bioelectrochem. Bioenerg.* **1987**, *18*, 211−217.
(45) Uysal, M.; Kutalp, G.; Ozdermirler, G.; Aykac, G. Ethanol-Induced Changes in Lipid Peroxidation and Glutathione Content in Rat Brain. *Drug Alcohol Depend.* **1989**, *23*, 227−230.
(46) Udenfriend, S.; Clark, C. T.; Axelrod, J.; Brodie, B. B. Ascorbic Acid in Aromatic Hydroxylation. *J. Biol. Chem.* **1954**, *208*, 731−738.
(47) Chen, J.-C.; Crino, P. B.; Schnepper, P. W.; To, A. C. S.; Volicer, L. Increased Serotonin Efflux by a Partially Oxidized Serotonin: 4,5-Diketotryptamine. *J. Pharmacol. Exp. Ther.* **1989**, *250*, 141−148.
(48) Cai, P.; Snyder, J. K.; Chen, J.-C.; Fine, R.; Volicer, L. Preparation, Reactivity, and Neurotoxicity of Tryptamine-4,5-Dione. *Tetrahedron Lett.* **1990**, *31*, 969−972.
(49) *Sadtler Standard Nuclear Magnetic Resonance Spectra*; Sadler Research Laboratories: Spring Garden, PA, 1977; Vol. 41−42, 25662M.

JM9504870